



HAL
open science

Central X-Ray Point Sources Found to Be Abundant in Low-mass, Late-type Galaxies Predicted to Contain an Intermediate-mass Black Hole

Alister Graham, Roberto Soria, Benjamin Davis, Mari Kolehmainen, Thomas Maccarone, James Miller-Jones, Christian Motch, Douglas Swartz

► **To cite this version:**

Alister Graham, Roberto Soria, Benjamin Davis, Mari Kolehmainen, Thomas Maccarone, et al.. Central X-Ray Point Sources Found to Be Abundant in Low-mass, Late-type Galaxies Predicted to Contain an Intermediate-mass Black Hole. *The Astrophysical Journal*, 2021, 923 (2), pp.246. 10.3847/1538-4357/ac34f4 . hal-03518762

HAL Id: hal-03518762

<https://hal.science/hal-03518762>

Submitted on 12 Jan 2022

HAL is a multi-disciplinary open access archive for the deposit and dissemination of scientific research documents, whether they are published or not. The documents may come from teaching and research institutions in France or abroad, or from public or private research centers.

L'archive ouverte pluridisciplinaire **HAL**, est destinée au dépôt et à la diffusion de documents scientifiques de niveau recherche, publiés ou non, émanant des établissements d'enseignement et de recherche français ou étrangers, des laboratoires publics ou privés.



Distributed under a Creative Commons Attribution 4.0 International License



Central X-Ray Point Sources Found to Be Abundant in Low-mass, Late-type Galaxies Predicted to Contain an Intermediate-mass Black Hole

Alister W. Graham¹ , Roberto Soria^{2,3} , Benjamin L. Davis^{1,4} , Mari Kolehmainen⁵, Thomas Maccarone⁶, James Miller-Jones⁷ , Christian Motch⁵ , and Douglas A. Swartz⁸

¹ Centre for Astrophysics and Supercomputing, Swinburne University of Technology, Victoria 3122, Australia; AGraham@swin.edu.au

² College of Astronomy and Space Sciences, University of the Chinese Academy of Sciences, Beijing 100049, People's Republic of China

³ Sydney Institute for Astronomy, School of Physics A28, The University of Sydney, Sydney, NSW 2006, Australia

⁴ Center for Astro, Particle, and Planetary Physics (CAP³), New York University, Abu Dhabi

⁵ Observatoire Astronomique, Université de Strasbourg, CNRS, UMR 7550, 11 Rue de l'Université, F-67000 Strasbourg, France

⁶ Department of Physics and Astronomy, Texas Tech University, Box 41051, Lubbock, TX 79409-1051, USA

⁷ International Centre for Radio Astronomy Research, Curtin University, GPO Box U1 987, Perth, WA 6845, Australia

⁸ Astrophysics Office, NASA Marshall Space Flight Center, ZP12, Huntsville, AL 35812, USA

Received 2021 August 16; revised 2021 October 12; accepted 2021 October 28; published 2021 December 28

Abstract

Building upon three late-type galaxies in the Virgo cluster with both a predicted black hole mass of less than $\sim 10^5 M_\odot$ and a centrally located X-ray point source, we reveal 11 more such galaxies, more than tripling the number of active intermediate-mass black hole candidates among this population. Moreover, this amounts to a $\sim 36 \pm 8\%$ X-ray detection rate (despite the sometimes high, X-ray-absorbing, H I column densities), compared to just $10 \pm 5\%$ for (the largely H I-free) dwarf early-type galaxies in the Virgo cluster. The expected contribution of X-ray binaries from the galaxies' inner field stars is negligible. Moreover, given that both the spiral and dwarf galaxies contain nuclear star clusters, the above inequality appears to disfavor X-ray binaries in nuclear star clusters. The higher occupation, or rather detection, fraction among the spiral galaxies may instead reflect an enhanced cool gas/fuel supply and Eddington ratio. Indeed, four of the 11 new X-ray detections are associated with known LINERs or LINER/H II composites. For all (four) of the new detections for which the X-ray flux was strong enough to establish the spectral energy distribution in the Chandra band, it is consistent with power-law spectra. Furthermore, the X-ray emission from the source with the highest flux (NGC 4197: $L_X \approx 10^{40} \text{ erg s}^{-1}$) suggests a non-stellar-mass black hole if the X-ray spectrum corresponds to the “low/hard state”. Follow-up observations to further probe the black hole masses, and prospects for spatially resolving the gravitational spheres of influence around intermediate-mass black holes, are reviewed in some detail.

Unified Astronomy Thesaurus concepts: X-ray point sources (1270); Spiral galaxies (1560); Intermediate-mass black holes (816)

1. Introduction

While galaxies suspected of harboring a supermassive black hole (SMBH) with a mass of around 10^5 – $10^6 M_\odot$ have long been identified (e.g., Filippenko & Sargent 1985; Ho et al. 1995; Greene & Ho 2007; Reines et al. 2013; Yuan et al. 2014; Graham & Scott 2015; Subramanian et al. 2016; Liu et al. 2018)—including POX 52 (Barth et al. 2004; Thornton et al. 2008), NGC 4395 (La Franca et al. 2015; den Brok et al. 2015; Brum et al. 2019), and NGC 404 (Davis et al. 2020)—there is an observational dearth of centrally located black holes with masses that are intermediate between stellar-mass black holes ($\lesssim 10^2 M_\odot$) and SMBHs ($\gtrsim 10^5 M_\odot$). Several late-type galaxies in the Virgo cluster are known to possess an active galactic nucleus (AGN), including Seyferts (e.g., NGC: 4388; 4569; 4579; 4639; and 4698) and LINERs (e.g., NGC 4438, NGC 4450, and NGC 4548). However, if the low Eddington ratios associated with the SMBHs of these AGN are representative of the mean, they warn that the X-ray luminosities of potential intermediate-mass black holes (IMBHs) in lower-mass spiral galaxies will be challenging to observe.

Traditional optical searches for low-mass AGN using spectroscopic line ratios in the Baldwin-Phillips-Terlevich (BPT: Baldwin et al. 1981) diagram, or the $W_{\text{H}\alpha}$ versus $[\text{N II}]/\text{H}\alpha$ (WHAN: Cid Fernandes et al. 2011) diagram, are limited given that the faint AGN signal is expected to be dwarfed by the stellar signal. Moreover, the hardening of the AGN spectral energy distribution (SED) in low-mass AGN can change the ionization structure, rendering the familiar line diagnostics less effective (Cann et al. 2019) and further contributing to why less than 1% of low-mass galaxies have been reported to have evidence of an AGN (Reines et al. 2013). In addition, studies at radio wavelengths are not ideal given that half of the X-ray luminous AGN are radio quiet (Radcliffe et al. 2021). However, members of the elusive population of IMBHs (10^2 – $10^5 M_\odot$) are starting to be found, with exciting discoveries in SDSS J160531.84 +174826.1 (Dong et al. 2007), HLX-1 in⁹ ESO 243-49 (Farrell et al. 2009), IRAS 01072+4954 (Valencia-S. et al. 2012), LEDA 87300 (Baldassare et al. 2015; Graham et al. 2016), NGC 205 (Nguyen et al. 2018, 2019), NGC 3319 (Jiang et al. 2018; Davis & Graham 2021), IC 750 (Zaw et al. 2020), and the host galaxies of GW170817A (Zackay et al. 2021), GW190521 (The LIGO Scientific Collaboration et al. 2020), and 3XMM J215022.4-055108 (Lin et al. 2020).

Original content from this work may be used under the terms of the [Creative Commons Attribution 4.0 licence](https://creativecommons.org/licenses/by/4.0/). Any further distribution of this work must maintain attribution to the author(s) and the title of the work, journal citation and DOI.

⁹ This is an off-center target.

Indeed, the flood gates may be about to open. Recently, Chilingarian et al. (2018) used the width and luminosity of the H α emission line to identify IMBH candidates at the centers of 305 galaxies: ten of which have X-ray data that reveal a coincident point source and suspected AGN. Four of these ten (which includes LEDA 87300) have a black hole mass estimate less than $\sim 10^5 M_\odot$. In addition, Moran et al. (2014) has reported on 28 nearby (< 80 Mpc) dwarf galaxies with narrow emission line (Type 2) AGN, while Mezcuca et al. (2018, Figure 1) report on X-ray emission coming from 40 predominantly star-forming dwarf galaxies with Type 2 AGN out to a redshift of ~ 1.3 , with three galaxies stretching the sample out to $z = 2.39$. (Mezcuca et al. 2018, Figure 8) applied a roughly linear $M_{\text{bh}}-M_{*,\text{gal}}$ relation to the galaxies’ stellar masses to predict that seven of their 40 galaxies have black hole masses less than $10^5 M_\odot$.

Closer to home, Graham & Soria (2019) and Graham et al. (2019, hereafter GSD19) have identified 63 Virgo cluster galaxies expected to house a central IMBH according to one or more black hole mass scaling relations, including the newer, morphology-dependent $M_{\text{bh}}-M_{*,\text{gal}}$ relations (Sahu et al. 2019a, and references therein). Reanalyzing the archival X-ray data for the 30 early-type galaxies in this set, Graham & Soria (2019) found that just three of them (IC 3442, IC 3492, and IC 3292)¹⁰ display a central X-ray point source.¹¹ In contrast, GSD19 reported that among the set of 33 late-type galaxies, three (NGC 4470, NGC 4713, and NGC 4178)¹² of the seven with archival X-ray data possessed a central X-ray point source.¹³

The higher activity ratio in the late-type spiral galaxies (3/7)—when compared to the dwarf early-type galaxies (3/30)—may have been an insightful clue. We have now obtained and analyzed Chandra X-ray Observatory (CXO) images for the remaining (33–7=) 26 previously unobserved late-type spiral galaxies. As will be reported here, nine of these 26 (or 12 of the original 33) late-type galaxies, contain a centrally located X-ray point source. This amounts to 36% of the late-type galaxy sample. The addition here of NGC 4212 and NGC 4492, both of which have centrally located X-ray point sources and are expected to house an IMBH, takes the sample of IMBH candidates to 14 (see Section 2). The probability that all 12 of these 33 (or 14 of 35) are stellar-mass X-ray binaries (XRBs) accreting near or above the Eddington ratio seems small¹⁴, and Occam’s razor favors that we are instead observing low Eddington ratio AGN, possibly due to the higher gas fractions keeping on the AGN pilot light. Indeed, star-forming galaxies are known to have AGN with a higher Eddington ratio than quiescent, i.e., non-star-forming galaxies (Kauffmann & Heckman 2009). Relatively inactive IMBHs in dwarf early-

type galaxies may, however, still be common (Silk 2017; Penny et al. 2018; Birchall et al. 2020).

In Section 2, we introduce a subsample of low-mass Virgo cluster spiral galaxies predicted to have an IMBH and reported here for the first time to have a centrally located X-ray point source. Results for the spiral galaxies with expected black hole masses greater than $10^5-10^6 M_\odot$ will be presented in a subsequent paper exploring AGN occupation fractions, Eddington ratios, and trends with the host galaxy mass. In Section 3, we report on the X-ray data for the subsample of active IMBH candidates, while Section 4 discusses the prospects for estimating the black hole mass using the X-ray data alone (Section 4.1) or when combined with radio data (Section 4.2). Section 4.3 addresses the issue of potential XRB contamination in more detail. In Section 5, we discuss expectations for spatially resolving the gravitational sphere of influence around IMBHs, and provide some direction for future observations of our, and other, IMBH candidates. Finally, Section 6 discusses dual and off-center AGN before a summary of our key findings is provided in Section 7.

2. The Sample and their Expected Black Hole Masses

2.1. The Sample

The abundance of SMBHs at the centers of galaxies has led to many black hole mass scaling relations, some of which were recently used by us to estimate the masses of the black holes at the centers of 100 early-type galaxies (Graham & Soria 2019) and 74 late-type galaxies (GSD19) in the Virgo galaxy cluster. The early-type galaxy sample was compiled by Côté et al. (2004) and the subsequent CXO images from the Large Project titled “The Duty Cycle of Supermassive Black Holes: X-raying Virgo” (PI: T.Treu, Proposal ID: 08900784) were used to identify which galaxies had AGN (Gallo et al. 2010). We have established a complementary CXO Large Project titled “Spiral galaxies of the Virgo Cluster” (PI: R.Soria, Proposal ID: 18620568) which has imaged 52 galaxies and utilized an additional (22+1=)¹⁵ 23 spiral galaxies for which suitable archival X-ray data existed.

The combined sample of 75 spiral galaxies is described in Soria et al. (2021), with an emphasis on the observations and data reduction, star formation rate measurements, and the identification of some 80 off-center ultraluminous X-ray sources (ULX: $L_{0.3-10\text{ keV}} \approx 10^{39}-10^{41} \text{ erg s}^{-1}$). Here, we are following up on GSD19, who determined that 33 of the original 74 spiral galaxies are expected to harbor a central IMBH. More precisely, this paper started with the (33–7=) 26 spiral galaxies predicted to have an IMBH but which did not previously have archival X-ray data.¹⁶ Of these 26 spiral galaxies, we focus on those found here to have a centrally located X-ray point source. We have discovered such sources in nine of these 26 galaxies, giving a hit rate of 12-from-33 when including the archival data. In addition, we have included NGC 4492 (not in the original sample of 74; see footnote 6) and NGC 4212 (already in the original sample of 74, but not counted in the subsample of 33), thereby taking the tally to 14-from-35. NGC 4212 has a potentially exciting dual central X-ray point source, and a predicted central black hole mass of $10^5-(2 \times 10^6)M_\odot$

¹⁰ X-ray point source discovery in IC 3442 and IC 3492 was by Gallo et al. (2010).

¹¹ None of the 30 have a compact radio source at 8.4 GHz, with a flux limit of 0.1 mJy (Capetti et al. 2009).

¹² X-ray point source discovery in NGC 4713 was by Terashima et al. (2015), and in NGC 4178 by Secrest et al. (2012).

¹³ While GSD19 noted that NGC 4178’s X-ray point source may be due to a stellar-mass black hole, they also noted that Satyapal et al. (2009) had reported a strong [Ne V] 14.32 μm emission line, with an ionization potential of 97.1 eV, indicative of an AGN.

¹⁴ Arguably, if there are no IMBHs, and the early-type galaxy sample implies that the probability of an XRB residing at the center of a galaxy is 3-from-30, or 1-in-10, then there is roughly a 4.7×10^{-5} probability (1-in-21000) of having a sample with as many as 12-from-33 galaxies with a central XRB. Taken from $\sum_{i=0}^{(33-12)} 0.1^{33-i} 0.9^i / (33-i)! i!$. The existence of XRBs with either a low- or high-mass donor star complicates this calculation and is addressed later in Section 4.3.

¹⁵ We have discovered a central X-ray point source in archival, Cycle 8, CXO data for NGC 4492, an additional Virgo spiral galaxy that is expected to harbor an IMBH, and which has taken our parent sample from 74 to 75 spiral galaxies.

¹⁶ The seven spiral galaxies which did have archival data were reported on in GSD19.

Table 1
IMBH Mass Predictions Based on the Host Galaxy Properties

Galaxy	D (Mpc)	$\log M_{\text{bh}} (M_{*,\text{total}})$	$\log M_{\text{bh}} (\phi)$	$\log M_{\text{bh}} (\sigma)$	$\log M_{\text{bh}} (M_{\text{nc}})$	$\overline{\log M_{\text{bh}}}$
Archival X-ray data presented in Graham et al. (2019)						
NGC 4178, VCC66	13.20 ± 3.00	3.9 ± 0.9	4.2 ± 1.6	3.1 ± 0.9	2.6 ± 1.6	3.5 ± 0.6
NGC 4713, ...	14.80 ± 3.55	3.8 ± 0.9	3.5 ± 1.9	2.8 ± 1.3	4.6 ± 1.7	3.6 ± 0.6
NGC 4470 ^a , VCC1205	16.40 ± 6.60	3.4 ± 1.2	4.6 ± 2.6	$5.1 \pm 0.8^{\text{b}}$	4.5 ± 1.7	4.6 ± 0.6
New X-ray data						
NGC 4197, VCC120	26.40 ± 3.92	4.3 ± 0.8	5.4 ± 0.9	4.8 ± 0.6
NGC 4212 ^c , VCC157	17.05 ± 2.62	6.0 ± 0.9	5.9 ± 0.4	5.1 ± 0.8	6.2 ± 1.6	5.8 ± 0.3
NGC 4298, VCC483	15.80 ± 2.54	5.3 ± 0.8	5.6 ± 0.8	4.2 ± 0.8	5.3 ± 1.7	5.1 ± 0.4
NGC 4313, VCC570	14.15 ± 2.92	4.9 ± 0.9	...	5.2 ± 0.8	6.7 ± 1.6	5.3 ± 0.6
NGC 4330, VCC630	19.30 ± 1.56	4.4 ± 0.8	4.4 ± 0.8
NGC 4405, VCC874	17.85 ± 3.32	4.4 ± 0.9	4.4 ± 0.9
NGC 4413 ^d , VCC912	16.05 ± 1.40	3.7 ± 0.8	4.5 ± 0.6	4.2 ± 0.5
NGC 4492 ^e , VCC1330	19.30 ± 3.54	4.9 ± 0.9	4.9 ± 0.9
NGC 4498, VCC1379	14.55 ± 3.62	3.7 ± 0.9	5.8 ± 1.8	...	3.8 ± 1.5	4.0 ± 0.7
NGC 4519, VCC1508	19.60 ± 8.48	4.2 ± 1.2	5.5 ± 2.3	4.5 ± 1.1
NGC 4607, VCC1868	19.70 ± 6.55	4.5 ± 1.1	4.5 ± 1.1

Notes. Column 2 displays the median redshift-independent distances from NED. Predicted black hole masses are in units of solar mass, derived from one to four independent observables (see Section 2.2) depending on their availability: total stellar mass, $M_{*,\text{total}}$; spiral arm pitch angle, ϕ ; central stellar velocity dispersion, σ ; and nuclear star cluster mass, M_{nc} . The final column provides the error-weighted, mean black hole mass, $\overline{\log M_{\text{bh}}}$.

^a Also known as NGC 4610.

^b Revised down from $10^6 M_{\odot}$ in GSD19 due to the velocity dispersion dropping from 90 to $\sim 60 \text{ km s}^{-1}$ (see Section 3.3.3).

^c Also known as NGC 4208.

^d Also known as NGC 4407.

^e NGC 4492 has archival CXO data, but is new in the sense that we did not report on the X-ray data in GSD19.

(GSD19), which is why it was not counted in the initial sample of 33 because this range is above $10^5 M_{\odot}$.

For the convenience of reference, all of these 14 galaxies with central X-ray point sources, and their predicted black hole masses, are presented in Table 1. The entries are explained in the following subsection. In a follow-up paper presenting the full sample of 75 galaxies, we will present the occurrence of a central X-ray point source with both the existence, or not, of a galaxy bar and also as a function of the disk inclination. Here, we simply report that among the 14 galaxies noted above, there is no preference for those with an X-ray point source to have a bar (six of 14 do) nor a particularly face-on orientation (nine of 14 have an axis ratio greater than 0.5).

In passing, it is relevant to again note that using powerful data mining techniques, Chilingarian et al. (2018) searched the CXO archives and identified a sample of 305 galaxies with both a Type I AGN, as determined from their optical spectra, and a suspected IMBH in the range $3 \times 10^4 < M_{\text{bh}}/M_{\odot} < 2 \times 10^5$. Ten of these galaxies were reported to have nuclear X-ray emissions, and four of these ten had a black hole mass estimated to be less than $10^5 M_{\odot}$. Of these four galaxies, and of relevance here, is that the one with the smallest black hole mass estimate is the Virgo Cluster Catalog dwarf galaxy VCC 1019 (SDSS J122732.18+075747.7) imaged by XMM-Newton. We downloaded and reprocessed the CXO data for VCC 1019—which is a background spiral galaxy at 150 Mpc (e.g., Grogin et al. 1998)—and found no X-ray emission, whereas Chilingarian et al. (2018) reported a “very faint” source. The nine (of ten) other galaxies with X-ray emission are not in the Virgo cluster.

2.2. The Predicted Black Hole Masses

We proceed under the hypothesis that (some of) the X-ray point sources are associated with massive black holes. There are now many approaches to predict a galaxy’s central black hole mass

which do not rely upon the assumption of stable (virialized) gas clouds orbiting the black hole in some universal geometrical configuration. That assumption employs a sample mean virial factor, $\langle f \rangle$, obtained by linking (reverberation mapping)-derived virial products (e.g., Peterson & Wandel 2000) to either the $M_{\text{bh}}-\sigma$ or $M_{\text{bh}}-M_{*,\text{gal}}$ relation defined by galaxies with directly measured black hole masses $\gtrsim 10^6 M_{\odot}$ (e.g., Onken et al. 2004; Graham et al. 2011; Bentz et al. 2009). In GSD19, we instead predicted the central black hole masses of our Virgo sample of spiral galaxies directly from the $M_{\text{bh}}-\sigma$ and $M_{\text{bh}}-M_{*,\text{gal}}$ relations for spiral galaxies, which have a total root mean square (and intrinsic) scatter of 0.63 (0.51 ± 0.04) and 0.79 (0.69) dex, respectively, in the $\log M_{\text{bh}}$ -direction. We additionally predicted the black hole mass using the host galaxy’s spiral arm pitch angle, ϕ , via the $M_{\text{bh}}-\phi$ relation that has a scatter of just 0.43 (0.30 ± 0.08) dex (Davis et al. 2017). We then highlighted galaxies for which multiple methods, from independent observations (σ , $M_{*,\text{gal}}$, ϕ), consistently yielded an expectation of an IMBH. Given the absence of bulges in some late-type spiral galaxies with massive black holes, and the somewhat comparable levels of scatter about the $M_{\text{bh}}-M_{*,\text{gal}}$ ($\Delta_{\text{rms,total}} = 0.79$ dex; Davis et al. 2018) and $M_{\text{bh}}-M_{*,\text{bulge}}$ ($\Delta_{\text{rms,total}} = 0.64-0.66$ dex; Davis et al. 2019) relations for spiral galaxies, we have not used the $M_{\text{bh}}-M_{*,\text{bulge}}$ relation.

In Table 1, the predicted black hole masses based on ϕ and σ are taken from GSD19. Due to our use of the median, rather than the mean, redshift-independent distance in the NASA/IPAC Extragalactic Database (NED)¹⁷, we have revised the predicted black hole masses from GSD19 that were based on the $M_{\text{bh}}-M_{*,\text{gal}}$ relation, and the mean redshift-independent distances. For each galaxy, we inspected the histogram of redshift-independent distances, and for some we removed outliers and rederived the median value, which is listed in

¹⁷ <http://nedwww.ipac.caltech.edu>

Table 1. The revised distances impact upon the absolute magnitudes and in turn the stellar mass of each galaxy, and thus the predicted black hole masses.

For reference, the nucleated Sérsic galaxy NGC 205 has the lowest directly measured black hole mass, $(7.1_{-5.3}^{+10.7}) \times 10^3 M_\odot$ (Nguyen et al. 2019, Table 6). With a stellar velocity dispersion of 33 km s^{-1} from HyperLeda¹⁸ (Paturel et al. 2003), NGC 205 agrees well with, and thus extends, the $M_{\text{bh}}-\sigma$ relation for Sérsic, and thus spiral galaxies into the $10^3-10^4 M_\odot$ range (Sahu et al. 2019b, Figures 3 and 11). The dwarf S0 galaxy NGC 404, with a reported black hole mass equal to $(7_{-2.0}^{+1.5}) \times 10^4 M_\odot$ (Nguyen et al. 2017), also follows the $M_{\text{bh}}-\sigma$ relation for Sérsic galaxies (Sahu et al. 2019b, Figures 2 and 3). Having a well-resolved nuclear star cluster, with a mass of $(1.8 \pm 0.8) \times 10^6 M_\odot$ (Graham & Spitler 2009; Nguyen et al. 2018), NGC 205 also agrees well with and extends the $M_{\text{bh}}-M_{\text{nc}}$ relation into this lower-mass range (Graham 2020).

2.2.1. Insight from Nuclear Star Clusters

For the nucleated galaxies, i.e., those with nuclear star clusters, we also include the estimate of the central black hole mass derived from the nuclear star cluster mass. As with massive black holes, the masses of nuclear star clusters have previously been discovered to correlate with their host spheroid’s mass (Balcells et al. 2003; Graham & Guzmán 2003). Furthermore, the coexistence of black holes and nuclear star clusters (Graham & Driver 2007; González Delgado et al. 2008; Seth et al. 2008; Graham & Spitler 2009; Graham 2016) implies the existence of a relation between black hole mass and nuclear star cluster mass, which is given by

$$\log\left(\frac{M_{\text{bh}}}{M_\odot}\right) = (2.62 \pm 0.42) \log\left(\frac{M_{\text{nc}}}{10^{7.83} M_\odot}\right) + (8.22 \pm 0.20) \quad (1)$$

(Graham 2016, 2020). This relation holds in the absence of a galaxy bulge, making it a useful tool for late-type spiral galaxies.

A nuclear star cluster is known to reside in a couple of our spiral galaxies with both (i) a central X-ray point source, and (ii) a suspected IMBH. The reported nuclear star cluster mass for NGC 4178 ($5 \times 10^5 M_\odot$; Satyapal et al. 2009) is assumed to have an accuracy of a factor of 2. Although Satyapal et al. (2009) report that NGC 4713 also contains a nuclear star cluster, or at least a point-like source (possibly contaminated by AGN light), they refrain from providing a mass measurement. In NGC 4498, the Johnson/Cousins Vband apparent magnitude of the nuclear star cluster has been reported as $21.53 \pm 0.02 \text{ mag}$ (Georgiev & Böker 2014), and the stellar mass for the nuclear star cluster has been taken as $(1.4 \pm 0.4) \times 10^6 M_\odot$ from Georgiev et al. (2016, Table A1). The expected black hole masses, based upon these nuclear star cluster masses, are calculated here using Equation (1), taken from Graham (2020, their Equation (7)), which is more accurate than the previous estimates obtained from the inverse of Equation (12) in GSD19. This $M_{\text{bh}}-M_{\text{nc}}$ relation is applicable¹⁹ for $10^5 \lesssim M_{\text{nc}}/M_\odot \lesssim 5 \times 10^7$, and has an

¹⁸ <http://leda.univ-lyon1.fr>

¹⁹ The upper mass cut (of $M_{\text{nc}} \lesssim 5 \times 10^7 M_\odot$) excludes systems with half-light radii greater than $\sim 20 \text{ pc}$, which may be regarded as nuclear disks rather than ellipsoidal-shaped star clusters.

uncertainty calculated using the expression

$$[\delta \log(M_{\text{bh}}/M_\odot)]^2 = \left[\log\left(\frac{M_{\text{nc}}}{10^{7.83} M_\odot}\right) \right]^2 (0.42)^2 + \left(\frac{2.62}{\ln 10}\right)^2 \left(\frac{\delta M_{\text{nc}}}{M_{\text{nc}}}\right)^2 + (0.20)^2 + (\delta_{\text{int}})^2, \quad (2)$$

where the intrinsic scatter within the $M_{\text{bh}}-M_{\text{nc}}$ relation, δ_{int} , has been taken to be 1.31 dex in the M_{bh} -direction (Graham 2020). The results are given in Table 1.

2.2.2. Error-weighted Mean Black Hole Masses

A novel approach employed by Davis & Graham (2021) in the case of NGC 3319 was to determine the error-weighted black hole mass from many independent estimates, $\log(M_{\text{bh},i})$. Accounting for each estimate’s associated uncertainty, $\delta \log(M_{\text{bh},i})$, the combined probability distribution function (PDF) yields the statistically most likely value (and its 1σ uncertainty range) for the black hole mass. When many such independent estimates are brought to bear on this derivation, as was the case for NGC 3319, one has a rather well-defined (Gaussian-like) PDF from which one can readily establish the probability of having detected an IMBH with $M_{\text{bh}} < 10^5 M_\odot$. Here, with fewer black hole estimates per galaxy than for NGC 3319, we proceed along a simpler path by determining the error-weighted mean of the logarithm of the black hole masses, such that

$$\overline{\log M_{\text{bh}}} = \frac{\sum_{i=1}^N w_i \log M_{\text{bh},i}}{\sum_{i=1}^N w_i}, \quad (3)$$

where we have used inverse-variance weighting²⁰ and thus $w_i = 1/(\delta \log M_{\text{bh},i})^2$. The 1σ standard error bar attached to this mean is calculated as

$$\delta \overline{\log M_{\text{bh}}} = \sqrt{\frac{1}{\sum_{i=1}^N w_i}}. \quad (4)$$

Table 1 provides the mean black hole mass estimates for our sample of late-type galaxies possessing a centrally located X-ray point source. With the exception of NGC 4212, with a dual X-ray point source, the estimates are typically less than $\sim 10^5 M_\odot$.

3. The X-Ray Data and Analysis

Readers not interested in the details of how the data was reduced (Sections 3.1 and 3.2), nor the individual results for each galaxy, may like to skip to Section 4 which describes the prospects for obtaining black hole masses from the X-ray data.

3.1. Nuclear Point-like Source Detection

CXO Advanced CCD Imaging Spectrometer (ACIS) data were obtained under the ‘‘Spiral galaxies of the Virgo Cluster’’ Large Project (Proposal ID: 18620568). In addition, we used archival observations for some of the galaxies. We analyzed the data in a consistent manner with GSD19, employing the Chandra Interactive Analysis of Observations (CIAO) Version

²⁰ This weighting gives the ‘‘maximum likelihood estimate’’ for the mean of the probability distributions under the assumption that they are independent and normally distributed with the same mean.

4.12 software package (Fruscione et al. 2006), and the Calibration Database Version 4.9.1. We reprocessed the event files of every observation with the CIAO task *chandra_repro*. For galaxies with multiple observations, we created merged event files with *reproject_obs*. In those cases, we used the stacked images to improve the signal-to-noise ratio in our search for possible nuclear sources; however, the fluxes from the nuclear candidates were then estimated from the individual exposures.

We used the coordinate position of the galactic nuclei reported in NED as a reference position for our search of nuclear X-ray sources. We looked for significant X-ray emission within $2''$ of the reference nuclear location. The fact that we knew in advance the (approximate) position of the sources we were looking for meant that we could identify significant detections with a far lower number of counts than we would require from a blind source-finding task (e.g., *wavdetect*). That, combined with the very low background level in the ACIS images, results in 99% significant detections even for sources with as few as 5 counts (e.g., see the Bayesian confidence intervals in Kraft et al. 1991). As a rough estimate, 5 ACIS-S counts in a typical 10 ks exposure, correspond to a 0.5–10 keV luminosity of $\sim 2 \times 10^{38}$ erg s $^{-1}$ at a distance of 17 Mpc.

When significant X-ray emission was detected at the nuclear position, we estimated whether the source was consistent with being point-like, or was instead significantly more extended than the instrumental point-spread-function (PSF) of the ACIS detector at that location (in most cases, close to the aimpoint of the S3 chip). In cases where we determined that the emission was extended, we inspected the images in the soft (0.3–1 keV), medium (1–2 keV), and hard (2–10 keV) bands separately. This enabled us to determine whether there was a point-like (harder) X-ray source surrounded by diffuse thermal emission, characteristic of star-forming regions; typically, the latter does not significantly contribute to the 2–10 keV band.

For all nuclear point-like sources, we defined source extraction regions with a radius suitable to the size of the PSF (typically, a circle with $2''$ radius for sources at the aimpoint of the S3 chip) and local background regions at least four times larger than the source region. We visually inspected all source and background regions to make sure they did not contain other contaminating sources. In all cases, we ran the CIAO task *srcflux* to estimate the absorbed and unabsorbed fluxes. The PSF fraction in the extraction circle was estimated with the *srcflux* option “psfmethod=arccorr,” which essentially performs a correction to infinite aperture. In some cases, when the count rate was high enough, we also extracted the source spectra and modeled them using the XSPEC (Arnaud 1996) package version 12.9.1, as described next.

3.2. Flux and Luminosity of Detected Nuclear Sources

The task *srcflux* provides two alternative estimates of the absorbed X-ray flux: model fluxes and model-independent fluxes. Both values can be described as approximations to the ideal “observed” flux that would be measurable from a data set with infinitely high signal-to-noise. For the model fluxes, we assumed a power-law spectrum with photon index $\Gamma = 1.7$ (Molina et al. 2009; Corral et al. 2011) and the Galactic line-of-sight column density of H I gas (HI4PI Collaboration et al. 2016), taken from the High Energy Astrophysics Science Archive Research Center (HEASARC).²¹ More realistically, even for nuclear sources

with the least amount of intrinsic absorption, we may expect a total N_{H} value which is a factor of 2 higher than the Galactic N_{H} value, owing to the absorbing matter in the host Virgo spiral galaxy plus that in the Milky Way. This conversion factor would depend on the size and morphological type of the host galaxy, on its metallicity and star formation rate, and on our viewing angle. However, the difference in the estimated unabsorbed luminosities corrected for a column density of, for example, $\sim 4 \times 10^{20}$ cm $^{-2}$, as opposed to $\sim 2 \times 10^{20}$ cm $^{-2}$ is only about 4% (well below the other observational and systematic uncertainties), because such column densities block photons only at the low end of the ACIS-S energy range, where the instrumental sensitivity is already very low. Thus, we avoided those complications, because they are largely irrelevant for the purpose of this work, and list the unabsorbed luminosities as corrected only for Galactic N_{H} in all cases when there are not enough counts for any significant estimate of $N_{\text{H,int}}$ (as explained later). It is simple to estimate the fluxes and luminosities of the same sources corrected for higher values of N_{H} (if so desired), with the Portable Interactive MultiMission Software (PIMMS)²².

Model-independent fluxes from *srcflux* are based on the energy of the detected photons, convolved by the detector response. For sources with a small number of counts, the detected photons may not uniformly sample the energy range, especially at higher energies (lower sensitivity): thus, the model-independent flux is not necessarily a more accurate approximation of the “ideal” observable flux than the model-dependent value. Moreover, we need the model-dependent fluxes in order to estimate the unabsorbed fluxes and luminosities, a conversion that cannot be done directly from the model-independent fluxes. In most cases in our sample of nuclear sources, the model-dependent and independent fluxes agree within the error bars. However, when they differ significantly, it is a clue that either our assumed power law is wrong, or that the H I column density is $>10^{20}$ cm $^{-2}$. We flagged those cases for further analysis with XSPEC.

In order to mitigate the effect of an uncertain N_{H} on our estimate of the unabsorbed flux and luminosity, we computed model-dependent fluxes with *srcflux* in the 1.5–7 keV band rather than in the “broad” 0.5–7 keV band. This is because photoelectric absorption is negligible above 1.5 keV, at least for the range of column densities seen in Virgo spirals (up to a few 10^{22} cm $^{-2}$). Thus, the observed count rate at 1.5–7 keV provides a more accurate normalization of the true power-law spectrum. We then compute the 0.5–7 keV flux by extrapolating the power-law model to lower energies.

There is a second reason why it is more convenient to use the 1.5–7 keV band rather than the full ACIS band for an estimate of the nuclear fluxes with *srcflux*. Some nuclei may have thermal plasma emission from diffuse hot gas (for example caused by star formation in the nuclear region) in addition to point-like emission from the potential central black hole. The spatial separation of the diffuse and point-like components is often impossible; two-component modeling is also not an option for low-count spectra from sources with luminosities $\lesssim 10^{40}$ erg s $^{-1}$ at the distance of the Virgo cluster. Instead, it is plausible to assume that the power-law component from the nuclear black hole dominates above 1.5 keV, and the ~ 0.5 keV thermal plasma emission affects mostly the softer band. Thus,

²¹ <https://heasarc.gsfc.nasa.gov/cgi-bin/Tools/w3nh/w3nh.pl>

²² <http://asc.harvard.edu/toolkit/pimms.jsp>

Table 2
CXO Point Sources Expected to have $M_{\text{bh}} \lesssim 10^5 M_{\odot}$

Galaxy NGC#	Obs. Date	Exp. ksec	$F_{0.5-7 \text{ keV}}$ mod-indpt	$F_{0.5-7 \text{ keV}}$ mod-dept	$N_{\text{H,Galaxy}}$ 10^{20} cm^{-2}	$L_{0.5-8 \text{ keV}}$ $10^{38} \text{ erg s}^{-1}$	$N_{\text{H,intrin}}$ 10^{22} cm^{-2}	Γ	kT_{in} keV	$L_{0.5-10 \text{ keV}}$ $10^{38} \text{ erg s}^{-1}$	$L_{2-10 \text{ keV}}$ $10^{38} \text{ erg s}^{-1}$
Presented in Graham et al. (2019)											
4178	2011-02-19	36.29	$0.50^{+0.16}_{-0.12}$	$0.56^{+0.25}_{-0.16}$	2.66	$4.04^{+16.86}_{-2.30}$	$0.47^{+0.50}_{-0.35}$	$3.43^{+1.66}_{-1.24}$...	$4.06^{+16.94}_{-2.31}$	$0.51^{+2.12}_{-0.29}$
4178	2011-02-19	36.29	$0.50^{+0.16}_{-0.12}$	$0.56^{+0.25}_{-0.16}$	2.66	$1.52^{+1.25}_{-0.56}$	$0.15^{+0.33}_{-0.15}$...	$0.56^{+0.35}_{-0.19}$	$1.52^{+1.25}_{-0.56}$	$0.35^{+0.30}_{-0.13}$
4713	2003-01-28	4.90	$1.17^{+0.74}_{-0.52}$	$1.52^{+0.91}_{-0.66}$	1.87	$4.40^{+2.62}_{-1.92}$...	1.7	...	$4.94^{+2.94}_{-2.15}$	$3.19^{+1.90}_{-1.39}$
4470 ^a	2010-11-20	19.78	$0.42^{+0.47}_{-0.33}$	$0.35^{+0.28}_{-0.20}$	1.60	$1.31^{+1.09}_{-0.74}$...	1.7	...	$1.47^{+1.23}_{-0.83}$	$0.95^{+0.79}_{-0.64}$
New X-ray data											
4197	2018-07-27	7.96	$11.20^{+2.40}_{-2.36}$	$10.60^{+3.20}_{-1.40}$	1.52	119^{+55}_{-31}	$0.35^{+0.72}_{-0.35}$	$1.24^{+0.84}_{-0.69}$...	144^{+66}_{-38}	113^{+53}_{-29}
4212 ^a	2017-02-14	14.86	$0.43^{+0.36}_{-0.24}$	$0.49^{+0.41}_{-0.27}$	2.67	$1.90^{+1.58}_{-1.03}$...	1.7	...	$2.13^{+1.78}_{-1.15}$	$1.38^{+1.14}_{-0.75}$
4298	2018-04-09	7.81	$2.68^{+1.54}_{-1.13}$	$1.84^{+1.04}_{-0.76}$	2.62	$6.10^{+3.46}_{-2.51}$...	1.7	...	$6.85^{+3.89}_{-2.82}$	$4.42^{+2.51}_{-1.82}$
4313 ^a	2018-04-14	7.96	$0.55^{+0.51}_{-0.32}$	$0.87^{+0.77}_{-0.48}$	2.40	$2.32^{+2.03}_{-1.29}$...	1.7	...	$2.61^{+2.28}_{-1.45}$	$1.68^{+1.47}_{-0.93}$
4330	2018-04-16	7.96	$6.30^{+2.35}_{-1.90}$	$6.55^{+2.70}_{-2.08}$	2.07	$80.7^{+48.6}_{-31.7}$	$4.33^{+2.86}_{-1.96}$	1.7	...	$90.6^{+54.6}_{-35.6}$	$58.5^{+35.2}_{-23.0}$
4405	2018-04-09	7.96	$0.62^{+0.57}_{-0.36}$	$0.84^{+0.76}_{-0.48}$	2.17	$3.54^{+3.22}_{-2.03}$...	1.7	...	$3.98^{+3.61}_{-2.28}$	$2.57^{+2.33}_{-1.48}$
4413	2018-05-10	7.80	$0.36^{+0.33}_{-0.22}$	$1.00^{+0.84}_{-0.54}$	2.32	$3.41^{+2.85}_{-1.84}$...	1.7	...	$3.83^{+3.76}_{-2.07}$	$2.47^{+2.07}_{-1.33}$
4492 ^a	2007-02-22	4.89	$0.69^{+0.63}_{-0.40}$	$1.31^{+1.01}_{-0.66}$	1.43	$6.77^{+6.58}_{-3.58}$	$0.05^{+0.25}_{-0.05}$	1.7	...	$7.60^{+7.39}_{-4.02}$	$4.91^{+4.77}_{-2.60}$
4492 ^a	2014-04-25	29.68	$0.54^{+0.50}_{-0.22}$	$0.85^{+0.46}_{-0.34}$	1.43	$4.40^{+2.81}_{-1.89}$	$0.05^{+0.25}_{-0.05}$	1.7	...	$4.94^{+3.16}_{-2.12}$	$3.19^{+2.94}_{-1.57}$
4498	2018-04-07	8.09	$0.60^{+0.44}_{-0.30}$	$1.17^{+0.85}_{-0.57}$	2.25	$3.29^{+2.37}_{-1.62}$...	1.7	...	$3.69^{+2.67}_{-1.81}$	$2.39^{+1.71}_{-1.18}$
4519	2018-05-05	8.45	$1.10^{+0.69}_{-0.49}$	$1.39^{+0.89}_{-0.61}$	1.36	$7.02^{+4.44}_{-3.12}$...	1.7	...	$7.88^{+4.99}_{-3.50}$	$5.09^{+3.22}_{-2.26}$
4607	2018-05-09	7.96	$4.93^{+2.22}_{-1.92}$	$3.84^{+2.20}_{-1.59}$	2.53	$51.0^{+49.3}_{-26.3}$	$4.68^{+5.86}_{-2.64}$	1.7	...	$57.3^{+55.3}_{-29.6}$	$37.9^{+34.8}_{-20.0}$

Note. Column 1: Galaxy name. ^a For galaxies with a dual X-ray point source, we are reporting the flux from the more central source. Column 4: the observed, i.e., partially absorbed, model-independent photon flux is for the centrally located X-ray point source in the CXO/ACIS-S 0.5–7 keV bands. The units are $10^{-14} \text{ erg cm}^{-2} \text{ s}^{-1}$, and the associated uncertainties show the 90% confidence range. Column 5: Absorbed model-dependent flux in units of $10^{-14} \text{ erg cm}^{-2} \text{ s}^{-1}$. Column 6: Galactic column density of neutral atomic hydrogen, H I. Column 7: The X-ray luminosity $L_{0.5-8 \text{ keV}}$ represents the unabsorbed 0.5–8 keV luminosity of each point source, derived using the distances provided in Table 1 and corrected for our Galaxy’s obscuring H I plus (when indicated in column 8) the obscuring line of sight H I intrinsic to the external galaxy. Column 9: The measured or adopted X-ray SED power-law slope, Γ . Column 10 gives the blackbody temperature of the model’s inner disk (*diskbb*). Column 11: Unabsorbed X-ray luminosity $L_{0.5-10 \text{ keV}}$ from 0.5–10 keV based on the extrapolated power-law SED. Column 12: Similar to column 11 but from 2–10 keV.

by normalizing the power-law model to the 1.5–7 keV flux and extrapolating it down to lower energies, we obtain a more accurate estimate of the nuclear emission than if we fit the power-law model over the whole 0.5–7 keV range.

In Table 2, one can find the model-independent fluxes of all the sources, and the model-dependent fluxes and luminosities of the sources, computed with *srcflux*. We converted the unabsorbed 0.5–7 keV fluxes to unabsorbed luminosities in the same band assuming the distances reported in Table 1. Finally, we converted luminosities across different bands using PIMMS, with the assumed power-law model. With $\Gamma = 1.7$, one has that $L_{0.5-8 \text{ keV}} = 1.075 L_{0.5-7 \text{ keV}}$, and $L_{0.5-10 \text{ keV}} = 1.20 L_{0.5-7 \text{ keV}}$.

We carried out a full spectral analysis for those nuclear sources with a sufficient number of counts, and for sources in which our preliminary *srcflux* analysis and our inspection of the X-ray colors suggested evidence of a high absorbing column density. We extracted spectra and associated response and ancillary response files with the CIAO task *specextract*. We then regrouped the spectra to 1 count per bin with the task *grppha* from the FTOOLS software (Blackburn 1995), and modeled them in XSPEC version 12.9.1 (Arnaud 1996), using the Cash (1979) statistics. The count rate is generally too low for complex modeling; however, we can spot cases of high $N_{\text{H, intr}}$ and constrain its value even for sources with as low as a dozen counts, because those counts would all be recorded at energies $> 1 \text{ keV}$. The second parameter left free in our XSPEC fitting is the power-law normalization. In a few cases, we had enough counts to leave also the photon index as a free parameter; in most other cases, we fixed it at the canonical value of 1.7. In one case, NGC 4178, the best-fitting power-law model is very

steep (Table 2), and the disk-blackbody model *diskbb* provides a more physical (although statistically equivalent) fit. Finally, for the sources modeled in XSPEC, we determined the 90% confidence limits on their absorbed and unabsorbed model fluxes (and hence, on their unabsorbed luminosities) with the convolution model *cflux*.

3.3. Galaxies with Archived X-Ray Data Reported in GSD19

Three galaxies (NGC 4178, NGC 4713, and NGC 4470) from GDS19 had both archival X-ray data revealing a central X-ray point source and at least two estimates for $M_{\text{bh}} < 10^5 M_{\odot}$. NGC 4178 (GSD19, Figure 11) represents a somewhat edge-on counterpart to NGC 4713 (GSD19, Figure 13), for which some additional comments are provided next. In the case of NGC 4470, it was not the primary target of the past CXO observations, and as such it was always located several arcminutes from the aimpoint, resulting in a broadened Point-Spread Function (PSF) at this galaxy’s center. Below, we present the X-ray contours for NGC 4470, not previously shown in GSD19.

3.3.1. NGC 4178: Blackbody vs. Power Law

As noted, NGC 4178 was presented in GSD19. Attempts to fit a power-law model to the X-ray SED, with its rapid drop off from the soft to the hard energy band, resulted in an unrealistically steep slope (see Table 2). The X-ray SED was instead quite well fit with a blackbody disk model having an intrinsic temperature $T_{\text{intrinsic}} = 0.56^{+0.35}_{-0.19} \text{ keV}$. The inner-disk radius R_{in} associated with the *diskbb* fit is such that $R_{\text{in}} (\cos \theta)^{1/2} \approx 1.19 N_{\text{dbb}}^{1/2} d_{10}$. With N_{dbb}

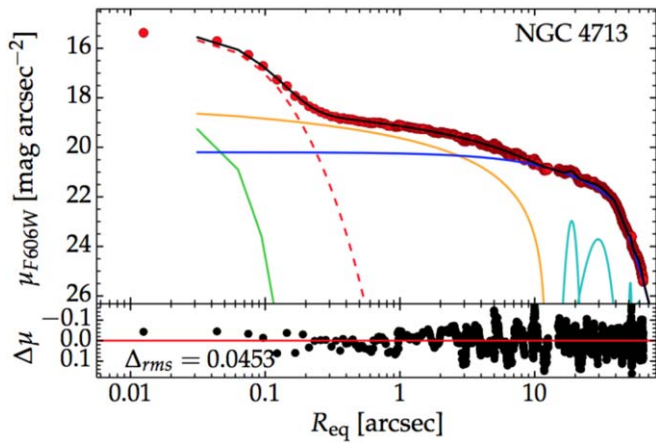


Figure 1. Geometric-mean axis, aka equivalent axis, light profile for the bulgeless galaxy NGC 4713, fit with a truncated exponential disk (dark blue) plus some faint spiral arm crossings (light blue), a bar (orange), a nuclear star cluster (dashed red), and a very faint point source (green).

the normalization of the *diskbb* model in *xspec*, d_{10} the distance to the source in units of 10 kpc, and θ our viewing angle ($\theta = 0$ is face-on), we obtain $R_{\text{in}}(\cos \theta)^{1/2} \approx 104$ km (53–613 km, 90% confidence).

We compared the power law and disk-blackbody models using the Anderson–Darling (AD) test statistics (e.g., Arnaud et al. 2011). Specifically, we performed Monte Carlo calculations of the goodness-of-fit in XSPEC, with the command *goodness*, and compared the percentage of simulations with the test statistic less than that for the data. For the power-law model, 75% of the realizations were better than the AD test value for the data (log AD = -3.67). For the disk-blackbody model, 43% of realizations were better than the AD value (log AD = -3.88). Thus, the disk-blackbody model is only weakly preferred. Moreover, Satyapal et al. (2009) have reported clear [Ne V] emission, indicative of an ionizing AGN, in NGC 4178.

3.3.2. NGC 4713: a LEDA 87300 Analog

Both the image of NGC 4713 (GSD19, Figure 13) and its light profile (Figure 1) resemble LEDA 87300 (Baldassare et al. 2015; Graham et al. 2016, Figures 2 and 5). From Hubble Space Telescope (HST) images, both galaxies can be seen to contain a central point source and a bar with spiral arms emanating from the ends (Baldassare et al. 2017). The better spatial resolution provided by HST has removed the uncertainty between the bar plus bulge components—collectively referred to as the “barge” (Graham et al. 2016)—that was previously affecting the ground-based images. Both galaxies now appear to be bulgeless. The centrally located point source in the optical image of LEDA 87300 may be partly due to its active galactic nucleus (AGN), which was bright enough to enable Ho et al. (1997) to flag this galaxy as having a “transition nucleus” with a luminosity-weighted [O I] strength intermediate between H II nuclei and LINERS (low-ionization nuclear emission-line regions). NGC 4713 was subsequently flagged by Decarli et al. (2007) as having a LINER/H II nucleus.

We have modeled the distribution of HST/WFC/ACS/F606W light in NGC 4713 following the process described in Davis et al. (2019). We used the *Isotfit* task (Ciambur 2015), run within the Image Reduction and Analysis Facility (IRAF)²³

package ELLIPSE to capture the galaxy light. We then modeled this using the PROFILER software (Ciambur 2016) and an empirical PSF (with airy rings) measured from a star. The result is shown in Figure 1.

We have found that NGC 4713 contains a slightly resolved nuclear star cluster with an equivalent-axis half-light radius equal to $0''.07$ (5 pc), a Sérsic index $n = 1.23$, and an *F606W* apparent magnitude of 19.57 ± 0.18 mag (AB mag). Correcting for 0.06 mag of Galactic extinction, and using a distance modulus of 30.85, one has an absolute magnitude of -11.34 mag (AB). Using an absolute magnitude for the Sun of $M_{\odot, F606W} = 4.72$ mag, and a stellar mass-to-light ratio²⁴ of 1.0 ± 0.5 , we obtain $\log(M_{\text{nc}}/M_{\odot}) = 6.43 \pm 0.31$ and a predicted black hole mass $\log(M_{\text{bh}}/M_{\odot}) = 4.56 \pm 1.66$ from Equation (1).

A point source for AGN light was additionally included in the modeling, but we were not able to obtain a useful constraint. Removal of the point source shown in Figure 1 brightens the star cluster by 0.01 mag. If the AGN point source is brighter than that shown, then the nuclear star cluster will be fainter and the predicted black hole mass will be smaller. This may explain why this prediction for the black hole mass is an order of magnitude higher than the predictions from the other methods (see Table 1), although the error bars are large. Finally, we note that -11.34 mag (AB) corresponds²⁵ to an *F606W* luminosity of 7.4×10^{39} erg s^{-1} , which is ~ 17 times brighter than the 0.5–8 keV X-ray luminosity. Should the IMBH candidate have $L_{\text{opt}} \approx L_{\text{X}}$, then the nuclear star cluster light will dominate the 606 nm continuum, as observed.

LEDA 87300 is of interest because of its AGN, evidenced by its nuclear X-ray point source, broad H α emission, and narrow emission line ratios (Baldassare et al. 2015). Using a virial f -factor of $2.3_{-0.6}^{+0.9}$ from Graham et al. (2011) gives a virial black hole mass of $2.9_{-2.3}^{+6.7} \times 10^4 f_{2.3} M_{\odot}$ in LEDA 87300 (Graham et al. 2016). The heightened uncertainty on the black hole mass, with its 1σ error range from 0.6×10^4 to 10^5 , is because the f -factor is the mean value derived from ~ 30 AGN with reverberation mappings, and when using this value to predict the virial black hole mass for an individual galaxy like LEDA 87300, in addition to the observational measurement errors, one needs to fold in the intrinsic scatter between the individual AGN, which is roughly a factor of 3, coming from the scatter in the $M_{\text{bh}}-\sigma$ diagram.

While LEDA 87300 has a stellar mass of $2.4 \times 10^9 M_{\odot}$ (accurate to a factor of 2) and an estimated stellar velocity dispersion of 40 ± 11 km s^{-1} (Graham et al. 2016, Section 3.2), NGC 4713 has a stellar mass of $4 \times 10^9 M_{\odot}$ (GSD19) and a measured velocity dispersion of 23.2 ± 8.9 km s^{-1} (Ho et al. 2009). We will endeavor to obtain optical spectra of NGC 4713 to detect a broad H α line. From this, we would be able to derive a virial mass for the black hole in NGC 4713 associated with the nuclear X-ray point source and LINER/H II nucleus. As noted in GSD19, the X-ray photons from the central point source in the archived CXO/ACIS-S image of NGC 4713 were detected in all three standard bands (soft, 0.3–1 keV; medium, 1–2 keV; hard, 2–7 keV), consistent with a power-law spectrum rather than purely a blackbody spectrum.

²⁴ Without a color for the nuclear star cluster, we note that the galaxy has a (Galactic absorption)-corrected color of $B_T - V_T = (12.19 - 0.101) - (11.72 - 0.077) = 0.446$, and $B_{F435W} - V_{F606W} = 0.446$ corresponds to $M/L_{F606W} = 0.98$ (Wilkins et al. 2013, Equation (2)).

²⁵ AB_{ν} [mag] = $-2.5 \log(f_{\nu} [\text{erg cm}^{-2} \text{s}^{-1} \text{Hz}^{-1}]) - 48.60$.

²³ <http://ast.noao.edu/data/software>

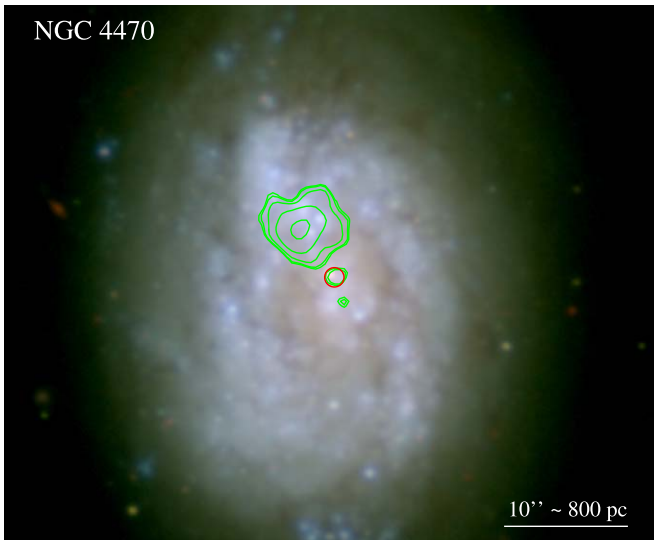


Figure 2. Next Generation Virgo Cluster Survey (NGVS; Ferrarese et al. 2012) image of NGC 4470, aka NGC 4610, (red = i filter; green = g ; blue = u^*), with Chandra/ACIS-S contours (0.5–7.0 keV band) overlaid in green. The contours are just a visual device to show the location of the X-ray source (accurate to $\approx 0''.6$). North is up, east is to the left. The red circle shows the NED-provided position for the galaxy’s optical nucleus, and it has a radius of $1''$ in this and subsequent figures, roughly reflecting the associated uncertainty/range coming from different galaxy isophotes.

3.3.3. NGC 4470: Dual X-Ray Point Sources 170 pc Apart

NGC 4470 (aka NGC 4610) is a face-on spiral galaxy (Figure 2). The Reference Catalog of galaxy Spectral Energy Distributions (RCSED; Chilingarian et al. 2017)²⁶ places NGC 4470 in the H II region of the narrow-line [O III]/H β versus [N II]/H α diagnostic diagram. However, it is becoming increasingly apparent that faint or “hidden” AGN can be missed when using BPT (Baldwin et al. 1981) diagnostic diagrams (e.g., Zezas et al. 2005; Sartori et al. 2015; Lamperti et al. 2017; Cann et al. 2019, 2021). This is perhaps not surprising in low-mass galaxies because, unless the Eddington ratio is high, the AGN signal in the central aperture/fiber/spaxel will be swamped by the galaxy’s starlight in these systems with low black hole masses (Mezcua & Domínguez Sánchez 2020). Although, by concentrating on a nearby ($D \leq 80$ Mpc) sample of dwarf galaxies, Moran et al. (2014) did find 28 galaxies dominated by narrow emission line (Type 2) AGN, and assuming an [O III]-to-bolometric luminosity correction factor of 1000 they reported minimum black hole masses of 10^3 – $10^6 M_{\odot}$ for their sample.

The RCSED reports a velocity dispersion of $61 \pm 6 \text{ km s}^{-1}$ for NGC 4470 (SDSS J122937.77+074927.1). This is lower than the value of $90 \pm 13.5 \text{ km s}^{-1}$ that was used in GSD19, and results in a lower $M_{\text{bh}-\sigma}$ derived black hole mass of $\log M_{\text{bh}} = 5.1 \pm 0.8$. This mass is now consistent (overlapping uncertainties) with the $M_{\text{bh}}-M_{*,\text{gal}}$ derived value of $\log M_{\text{bh}} = 4.1 \pm 1.0$ (GSD19).

Given that the pre-existing CXO data for NGC 4470 was (intentionally)²⁷ offset from the aimpoint of the telescope, it required a careful reanalysis. Six of the past seven ACIS observations (spanning 2010–2019) only captured the nuclear region of NGC 4470 on the external chips, where the PSF was

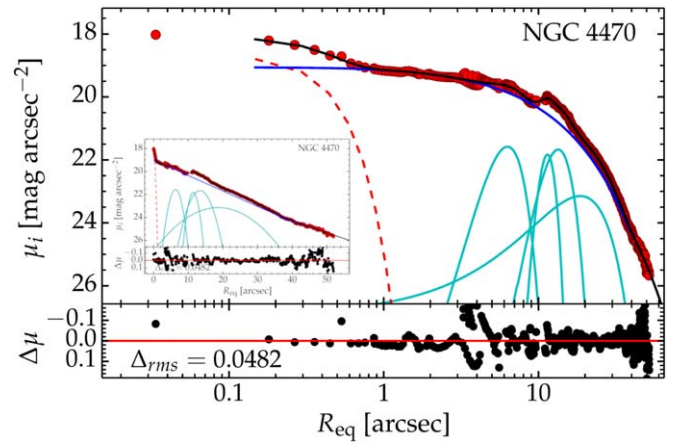


Figure 3. Similar to Figure 1, but for NGC 4470 (aka NGC 4610).

unfortunately too broad and distorted to obtain a reliable flux measurement. However, a ~ 20 ks exposure from 2010 (CXO Obs. ID 12978), directed 4 arcminutes away at the globular cluster RZ 2109 around NGC 4472, proved fruitful, and we have reanalyzed these data to report on NGC 4470’s central X-ray point source (Table 2). The galaxy’s optical center, as given by NED, coincides with a red feature which we cannot resolve in the NGVS image with $0''.7$ seeing. Figure 2 displays the overlapping X-ray point source at this central location. Both this X-ray source and the brighter source to the south proved too faint to acquire a spectrum.

Fitting a point source to the CFHT/NGVS/ i -band data (see Figure 3) yields a luminosity for the star cluster of $\log L_i/L_{\odot,i} = 6.57 \pm 0.35$, based on $\mathfrak{M}_{\odot,i} = 4.58$. With an i -band mass-to-light ratio of 0.70 ± 0.04 , based on a galaxy $g-i$ color equal to 0.69 ± 0.03 and using the color-dependent stellar mass-to-light ratios from Roediger & Courteau (2015), the corresponding stellar mass of the nuclear star cluster is $\log M_{\text{nc}}/M_{\odot} = 6.42 \pm 0.35$, and the predicted black hole mass is $\log M/M_{\odot} = 4.53 \pm 1.72$ (Equation (1)). However, this may be an upper limit due to contamination by AGN light increasing the light that we have assigned to the star cluster. That is, we have effectively erred on the side of caution and are not under-predicting the black hole mass in an attempt to predict/find IMBHs. We also modeled the galaxy components in both the g - and i -band NGVS images, and we measured a $g-i$ color equal to 0.57 for the nuclear component. This resulted in a 23% smaller stellar-mass estimate for the star cluster, and a 50% smaller estimate for the black hole mass. Although, this color for the nuclear component may be influenced by AGN light and as such we have erred on the side of caution and adopted the former measurement.

There is another equally bright X-ray source $2''.1$ (170 pc) to the south, and a more extended source ($\sim 10^{39} \text{ erg s}^{-1}$) located $6''$ northeast of the nuclear position and associated with an excess of blue stars and ongoing star formation. Based on the location of the second X-ray point source, at 170 pc from the nucleus, it may be a stellar-mass ULX, but is potentially more interesting than that if it represents one half of a dual IMBH system. A longer CXO exposure with the aimpoint on NGC 4470 would enable this to be answered.

²⁶ <http://rcsed.sai.msu.ru/catalog>

²⁷ The primary CXO target was NGC 4472 and its halo.

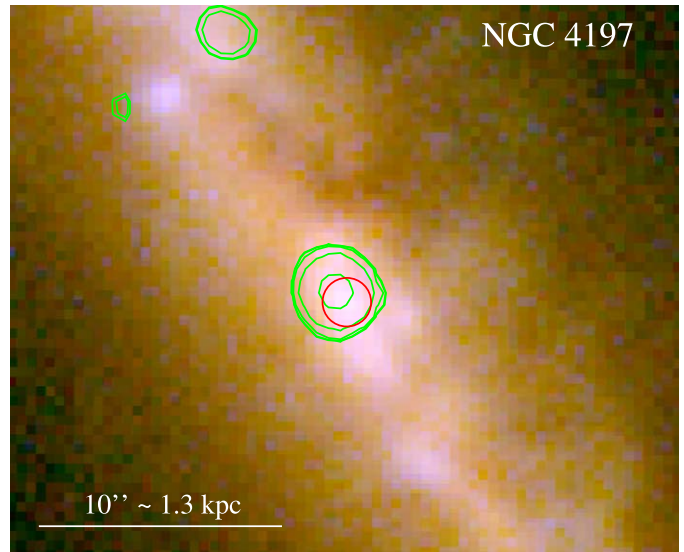
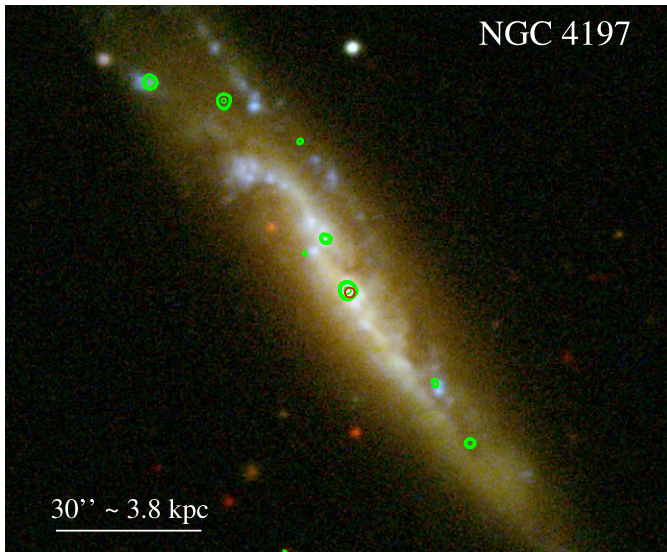


Figure 4. Left: similar to Figure 2, but displaying a Sloan Digital Sky Survey (SDSS Alam et al. 2015) image of NGC 4197 (red = i' filter; green = g' ; blue = u'). Right: zoom-in on the inner region.

3.4. Galaxies with New X-Ray Data

3.4.1. NGC 4197: a Likely Bright IMBH

As with NGC 4178 above, NGC 4197 appears in the flat galaxy catalog of Karachentsev et al. (1993) due to the somewhat edge-on (inclination = 79 degrees) orientation of its disk relative to our line of sight. Dahari (1985) has reported weak $H\alpha$ emission coming from the nucleus of this galaxy.

As a part of our Virgo cluster X-ray survey, NGC 4197 was observed by CXO for ≈ 8 ks, on 2017 July 26 (for more details, see Soria et al. 2021). We find a strong, point-like X-ray source (Figure 4) located at R.A. = $12^{\text{h}}14^{\text{m}}38^{\text{s}}59$, decl. = $+05^{\circ}48'21''2$ [J2000.0]. Considering the scatter in the positions reported by NED, this is consistent with the position of the optical nucleus: it is $\approx 0''.7$ (≈ 90 pc) away from the r -band SDSS position.

We extracted a spectrum within a $2''$ circular source region (see Figure 5), with the local background extracted from the annulus between radii of $3''$ and $9''$. We then fit the spectrum in XSPEC, using the Cash statistics. We find that the spectrum (Figure 5) is well described (C-statistic of 62.7 for 50 degrees of freedom) by a power law with photon index $\Gamma = 1.24^{+0.84}_{-0.69}$ and an intrinsic²⁸ column density $N_{\text{H}} = 3.5^{+7.2}_{-3.5} \times 10^{21} \text{ cm}^{-2}$. The unabsorbed 0.5–7 keV flux is $F_{0.5-7 \text{ keV}} = 1.1^{+0.3}_{-0.2} \times 10^{-13} \text{ erg cm}^{-2} \text{ s}^{-1}$. After correcting for absorption according to our best-fitting power-law model, we derive a luminosity $L_{0.5-10 \text{ keV}} = 1.4^{+0.7}_{-0.3} \times 10^{40} \text{ erg s}^{-1}$ at the assumed distance of 26.4 Mpc for this galaxy. If the X-ray spectrum corresponds to the low/hard state of an IMBH, the black hole mass would be \gtrsim a few 10^3 solar masses.

We also tried to fit the spectrum with a disk-blackbody model. We rule out a peak disk temperature $T_{\text{in}} \lesssim 1.6$ keV at the 90% confidence levels. Models with disk temperatures higher than that are acceptable (and, for $T_{\text{in}} \gtrsim 3$ keV, essentially identical to the power-law model) because the peak emission moves close to or beyond the Chandra band, and we

²⁸ By “intrinsic”, we are referring to the intervening number density beyond our Galaxy, primarily within the external galaxy.

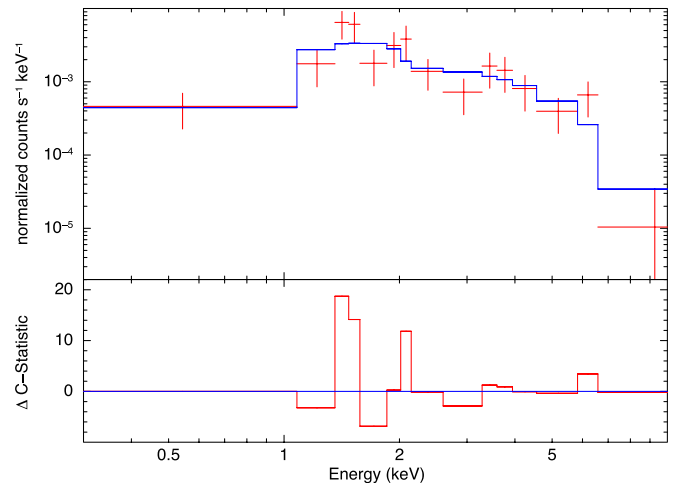


Figure 5. CXO/ACIS-S spectrum of the nuclear source in NGC 4197, fit with a power-law model. The data points have been grouped to a signal-to-noise >1.8 for plotting purposes only. The fit was done on the individual counts, using Cash statistics. See Section 3.4.1 for the fit parameters.

are only seeing the power-law-like section of the disk-blackbody below its peak. Disk temperatures of up to ~ 2 keV are sometimes seen in stellar-mass ULXs with a supercritical disk (slim disk). Thus, we cannot rule out that the source is a $\approx 10^{40} \text{ erg s}^{-1}$ stellar-mass ULX (e.g., Bachetti et al. 2014) located exactly at the nuclear position, but the simplest explanation consistent with the data is that it is the nuclear BH of this galaxy.

The Eddington luminosity can be expressed as $L_{\text{Edd}} \approx 1.26 \times 10^{38} (M_{\text{bh}}/M_{\odot})(\sigma/\sigma_{\text{T}})^{-1} \text{ erg s}^{-1}$. Given that NGC 4197 has $L_{0.5-10 \text{ keV}} = 144 \times 10^{38} \text{ erg s}^{-1}$, and assuming there is a hydrogen plasma with $\sigma = \sigma_{\text{T}}$ (the Thomson scattering cross section), this luminosity equates to a $\sim 10^2 M_{\odot}$ black hole accreting at the Eddington limit, or a $\sim 10 M_{\odot}$ black hole accreting at ten times the Eddington limit. Alternatively, given that we have predicted $\log M_{\text{bh}} = 4.8 \pm 0.6$ for NGC 4197 (Table 1), the Eddington luminosity for such a black hole is

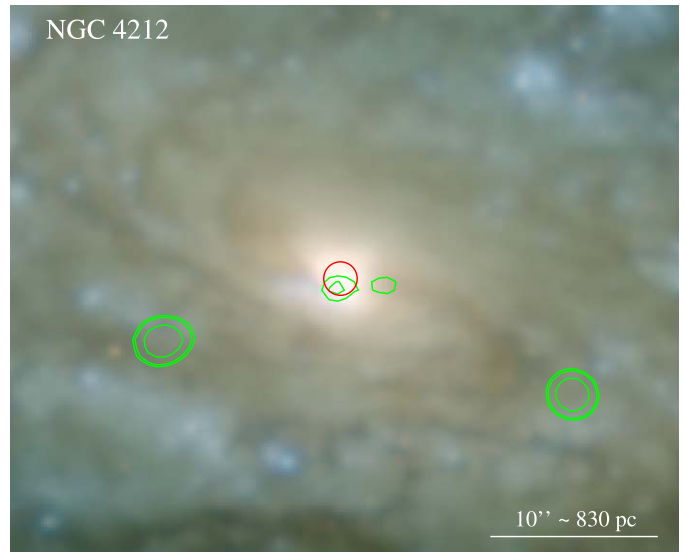
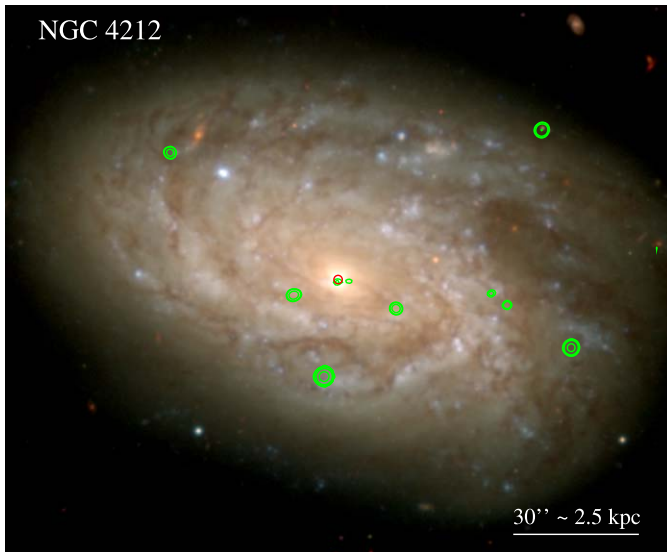


Figure 6. Similar to Figure 4, but displaying an NGVS image of NGC 4212 (aka NGC 4208).

$8.2^{+24.5}_{-6.1} \times 10^{42} \text{ erg s}^{-1}$. Expressing the Eddington ratio as L_X/L_{Edd} , with $L_X \equiv L_{0.5-10 \text{ keV}}$, implies an Eddington ratio of 0.0018, or 0.18%.

3.4.2. NGC 4212: Dual X-Ray Point Sources 240 pc Apart

Decarli et al. (2007) report that NGC 4212 (aka NGC 4208) is a LINER/H II composite galaxy. Filho et al. (2002, Table 1) searched for, but did not detect, a radio point source in this galaxy which Sérsic (1973) noted had a peculiar amorphous nucleus, likely due to dust. Scarlata et al. (2004) report dust absorption almost down to the center of the HST/STIS *R*-band image, but they show a noticeable brightening within the core which is also evident in the NICMOS/F190N image from HST observing program 11080 (P.I.: D. Calzetti).

NGC 4212 is the only galaxy in our list of 14 spiral galaxies to have a predicted black hole mass greater than $\approx 10^5 M_\odot$, weighing in at $6^{+7}_{-3} \times 10^5 M_\odot$. However, it is particularly interesting and worthy of inclusion because we have discovered that there are *two* faint CXO sources near the nucleus, with one of them displaced by a little less than $1''$ from the optical nucleus. Considering the positional uncertainty at such faint levels, and the presence of a dust lane likely shifting the optical center northward, this X-ray point source may be consistent with the optical nucleus.²⁹ The second, nearby, X-ray point source is $2''.9$ (≈ 240 pc) away. Their separation is resolvable with CXO (see Figure 6). As with NGC 4470, this off-center X-ray point source could be an XRB.

It is tempting to investigate the archived HST image of this galaxy in order to get at the galaxy’s nuclear star cluster magnitude and mass. However, like the LINER/H II galaxy NGC 4713, we need to be mindful that this is also a LINER/H II galaxy, and as such some of the excess nuclear light will be optical emission emanating from the unresolved, nonthermal AGN, as is the case in, for example, the LINER galaxy NGC 4486 (Ferrarese et al. 2006) and the Seyfert 1.5 galaxy NGC 4151 (Onken et al. 2014, Figure 4). Modeling the HST/NICMOS/F190N image, we find the galaxy is well fit with a nuclear star cluster having a magnitude of 17.64 ± 0.75 (AB

mag) and a half-light radius of $0''.23$ (19 pc) (see Figure 7). For $\mathfrak{M}_{\odot, F190N} = 4.85$ and $M/L_{F190N} = 0.5 \pm 0.1$, this translates to a mass of $\log(M_{\text{nc}}/M_\odot) = 7.05 \pm 0.34$, from which one would predict a black hole mass of $\log(M_{\text{bh}}/M_\odot) = 6.2 \pm 1.6$, supportive of the expectation from the galaxy’s stellar mass and spiral arm pitch angle (see Table 1). As with the AGN in NGC 4713, we were unable to provide a useful constraint.

3.4.3. NGC 4298

Figure 8 presents the optical and X-ray image for NGC 4298, while Figure 9 provides a decomposition of the galaxy light as seen in the HST/WFC3/IR F160W image from HST observing program 14913 (P.I.: M. Mutchler).

Optical/near-IR nuclei in HST images may be active BHs and/or star clusters. Côté et al. (2006) showed that the nuclear star clusters in the Virgo cluster galaxies are slightly resolved with HST/ACS, enabling one to differentiate between point sources and the spatially extended star clusters. While HST’s spatial resolution is better in the UV and optical than it is in the near-IR—simply because of how the diffraction limit scales linearly with wavelength—NGC 4298 is too dusty to see the nucleus at UV/optical wavelengths. However, NGC 4298 is clearly nucleated at $1.6 \mu\text{m}$ (and also $1.9 \mu\text{m}$), and Figure 9 reveals that, using Profiler (Ciambur 2016), its nucleus can be well approximated by a Sérsic function (convolved with the HST’s PSF) plus a tentative detection of a faint point source. The Sérsic nucleus has a half-light radius equal to $0''.20$ (15 pc) and an apparent (absolute) AB magnitude of 18.1 ± 0.3 mag (-12.9 ± 0.5 mag) in the F160W band.³⁰ The tentative point source, representing the putative AGN, has an apparent (absolute) magnitude of 20.4 ± 0.3 mag (-10.6 ± 0.5 mag).

Using an absolute magnitude for the Sun of $\mathfrak{M}_{\odot, F160W} = 4.60$ mag (AB) (Willmer 2018), and $M/L_{F160W} = 0.5$, gives a nuclear star cluster mass $\log(M_{\text{nc}}/M_\odot) = 6.7 \pm 0.4$ and thus a predicted black hole mass of $\log(M_{\text{bh}}/M_\odot) = 5.3 \pm 1.7$ using Equations (1) and (2).

²⁹ The X-ray point source is too faint to establish whether or not it is moderately absorbed.

³⁰ Performing the decomposition without the point source yields an apparent magnitude for the star cluster of 17.9 ± 0.2 mag.

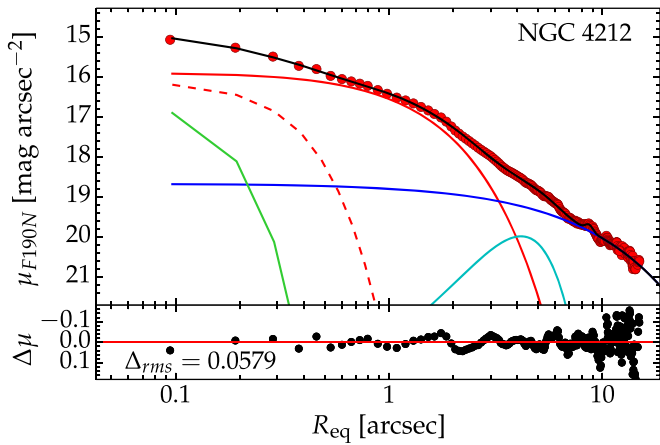


Figure 7. Similar to Figure 1, but for NGC 4212.

3.4.4. NGC 4313: Dual X-Ray Point Sources 590 pc Apart

Decarli et al. (2007) report that NGC 4313 is a Seyfert/LINER galaxy. From our CXO data, we report the discovery of an apparently faint, point-like, X-ray source coincident³¹ with the optical nucleus (Figure 10). Due to the galaxy’s somewhat edge-on orientation, it may have a high intrinsic absorption of X-ray photons. Just one of the six X-ray photons is in the 0.3–1 keV band, three are in the 1–2 keV band, and two are in the 2–10 keV band. Offset by $8''.4$ (590 pc) is a second, slightly fainter, X-ray point source.

We have been able to inspect an HST/NICMOS/F190N image from HST observing program: 11080 (P.I.: D. Calzetti) and decompose the galaxy light, which appears to consist of a bulge, plus a large-scale disk with a weak bar and ansae, and a nuclear star cluster with $m = 16.72 \pm 0.75$ (AB mag), Sérsic index $n \approx 0.8$ and effective half-light radius $R_e \approx 10$ pc (Figure 11). To obtain the mass of this nuclear component, we have used $M_{\odot, F190N} = 4.85$ mag (AB) (Willmer 2018), corrected for 0.011 mag of Galactic extinction, and assumed³² $M/L_{F190N} = 0.5 \pm 0.1$. This yields a stellar mass for the nuclear component of $\log(M_{nc}/M_{\odot}) = 7.27 \pm 0.36$, and this value may be an underestimate given that there will be some internal extinction at $1.9 \mu\text{m}$ coming from within the inclined galaxy NGC 4313. This leads to a higher than anticipated black hole mass prediction of $\log(M_{nc}/M_{\odot}) = 6.74 \pm 1.64$.

3.4.5. NGC 4330: $L_X \approx 10^{40} \text{ erg s}^{-1}$

NGC 4330 is experiencing ram pressure stripping of both its neutral HI gas (Chung et al. 2007; Abramson et al. 2011) and its ionized gas (Vollmer et al. 2012; Fossati et al. 2018).

The edge-on orientation of its disk to our line of sight, coupled with the detection of a nuclear X-ray source, suggests that it may harbor an intrinsically bright AGN given that some X-rays have penetrated their way through and out of the disk plane (see Figure 12). For comparison, NGC 4197 and NGC 4313 (Figures 4 and 10) and NGC 4178 (GSD19) represent other examples of spiral galaxies with somewhat edge-on disks in which we have detected a nuclear X-ray point source.

³¹ As with NGC 4212, a dust lane has likely shifted the optical nucleus of NGC 4313.

³² For reference, Barth et al. (2009) found an M/L_{F190N} value of 0.47 for the nucleus of the late-type Sd galaxy NGC 3621.

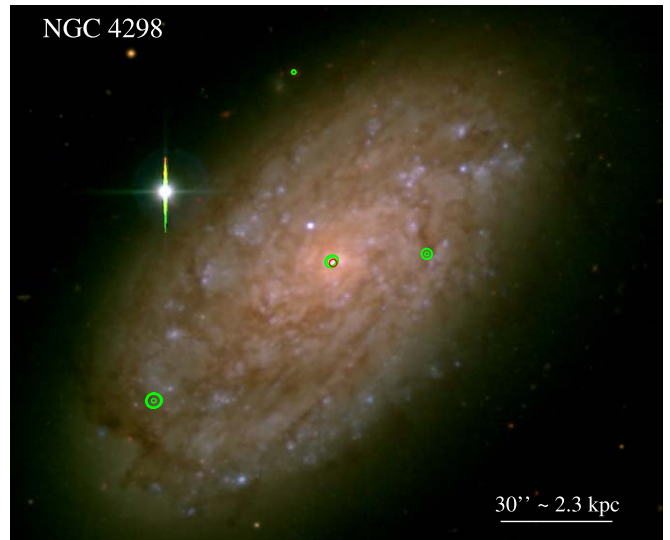


Figure 8. Similar to Figure 2, but displaying an NGVS image of NGC 4298.

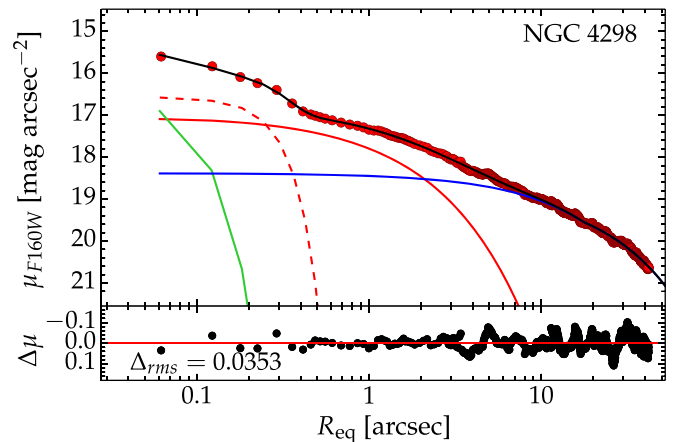


Figure 9. Similar to Figure 1, but for NGC 4298.

In NGC 4330, the CXO source is $\approx 2''$ from the optical center reported by NED. However, as Figure 12 shows, the location of the dust lane, coupled with the slight banana shape of the galaxy, may result in the optical centroid derived from the outer isophotes not corresponding to the true nucleus of the galaxy, which might instead be flagged by the location of the CXO source. Among our sample of galaxies expected to possess a central IMBH, NGC 4330 has the second brightest central X-ray point source, after NGC 4197 (see Table 2).

As with NGC 4197, we were able to obtain a meaningful X-ray spectrum from the central point source in NGC 4330 (see Figure 13). The background-subtracted spectrum was fit in XSPEC, using the Cash statistics, and is well described by a power law with a (fixed) photon index $\Gamma = 1.7$ and a high intrinsic column density, $N_H = 4.3^{+2.9}_{-2.0} \times 10^{22} \text{ cm}^{-2}$. The unabsorbed flux $F_{0.5-7 \text{ keV}} = 6^{+3}_{-2} \times 10^{-14} \text{ erg cm}^{-2} \text{ s}^{-1}$. At a distance of 19.30 Mpc, this corresponds to a luminosity $L_{0.5-7 \text{ keV}} = 1.727^{+0.645}_{-0.515} \times 10^{39} \text{ erg s}^{-1}$. Extrapolating the power law, one has $L_{0.5-10 \text{ keV}} = 0.9^{+0.6}_{-0.3} \times 10^{40} \text{ erg s}^{-1}$. Lehmer et al. (2010) report that nuclear X-ray luminosities $> 10^{40} \text{ erg s}^{-1}$ can confidently be ascribed to

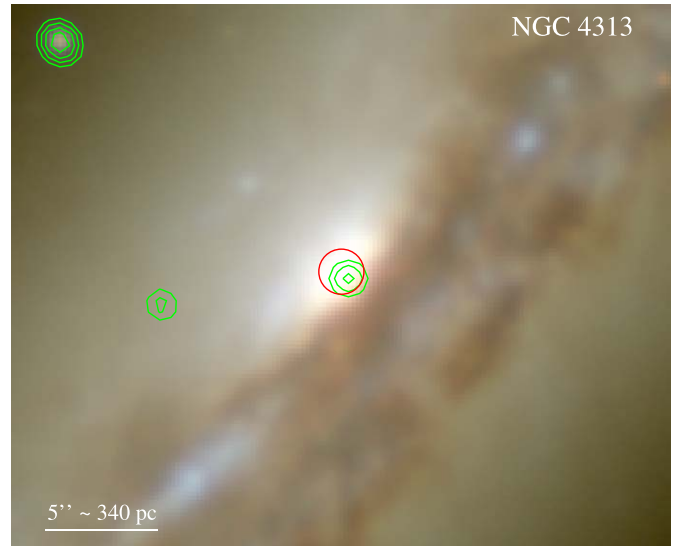
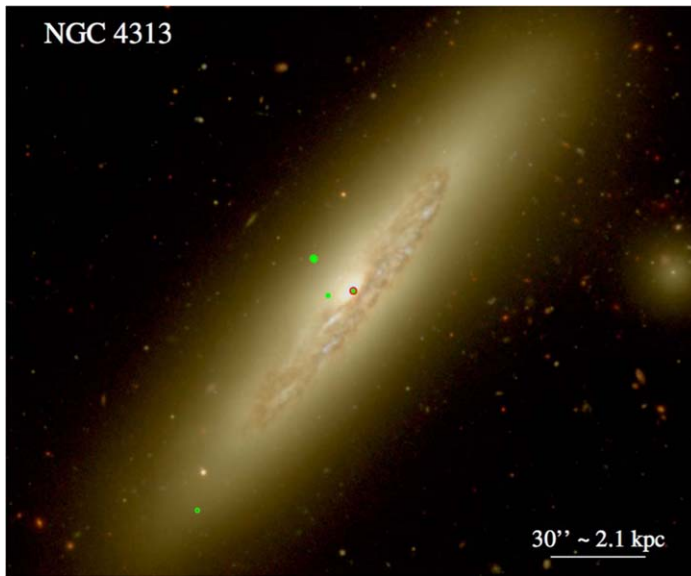


Figure 10. Similar to Figure 4, but displaying an NGV image of NGC 4313.

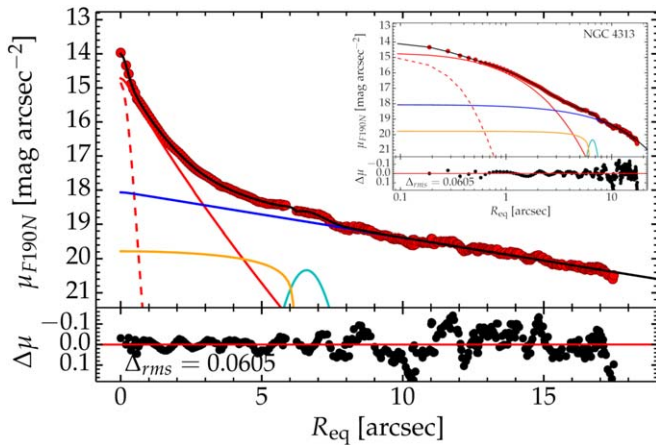


Figure 11. Similar to Figure 1, but for NGC 4313.

AGN emission, making NGC 4330, along with NGC 4197 ($L_{0.5-10 \text{ keV}} = 1.4 \times 10^{40} \text{ erg s}^{-1}$), strong candidates for IMBHs.

3.4.6. NGC 4405 and NGC 4413

NGC 4405 (Figure 14) and NGC 4413 (aka NGC 4407, see Figure 14) have fairly face-on disks. We have discovered a central X-ray point source in both, although neither is particularly strong. Their fluxes and luminosities are provided in Table 2.

3.4.7. NGC 4492; Dual X-Ray Point Sources 550 pc Apart

NGC 4492 is a new addition to the sample in GSD19, having useful CXO data from Cycle 8 (4.89 ks, Proposal 08700652, P.I.: S. Mathur) and Cycle 15 (29.68 ks, Proposal 15400260, P.I.: T. Maccarone), and an expected IMBH at its center based upon the galaxy’s stellar luminosity (see Table 1). Decarli et al. (2007) classified this galaxy as having no ($H\alpha$ nor $[NII]$) emission lines based upon their 2”-slit spectra from the Bologna Faint Object Spectrograph (BFOSC) attached to the Loiano 1.5 m telescope. However, we find that it possesses a

central X-ray point source, and a second X-ray point source 550 pc to the east of the nuclear point source (Figure 15).

We have combined the above two CXO exposures (using the CIAO task *specextract*, with the option “combine_spectra=yes”) to obtain the spectrum of the faint nuclear source at the center of NGC 4492. Figure 16 reveals a power-law SED, with $\Gamma = 1.7$, as opposed to the blackbody radiation curve of a hot accretion disk. After fitting this combined spectrum, we held N_H and Γ constant (see Table 2), leaving the normalization parameter free, and we fit the two individual spectra in XSPEC. The results are given in Table 2.

3.4.8. NGC 4498

NGC 4498 contains a few knots of star formation along its spine, as seen in HST observing program 5446 (P.I.: G. D. Illingworth, WFPC2/F606W). As noted in Section 2, Georgiev et al. (2016) have reported a stellar mass for the central star cluster of $(136_{-41}^{+46}) \times 10^4 M_\odot$ using a Vband mass-to-light ratio of $0.63_{-0.19}^{+0.21}$. Associated with this, we report the discovery of an X-ray point source (Figure 15).

3.4.9. NGC 4519

Globally, like NGC 4713, NGC 4519 (Figure 15) somewhat resembles the barred, bulgeless spiral galaxy LEDA 87300 (Baldassare et al. 2017). Centrally, NGC 4519 contains knots of star formation near its nucleus, and defining a single nuclear star cluster may prove problematic as there are multiple candidates seen in the HST images from observing program 9042 (P.I.: S. J. Smartt, F814W) and observing program 10829 (P.I.: P. Martini, F606W).

3.4.10. NGC 4607: $L_x \approx 0.6 \times 10^{40} \text{ erg s}^{-1}$

As with the edge-on galaxy NGC 4330, NGC 4607 is aligned edge-on to our line of sight. Given the expected high line-of-sight column density of neutral hydrogen through the disk of this galaxy, our discovery of a central X-ray source (Figure 15) suggests that it must be intrinsically bright and contain X-ray photons in the higher energy bands. While the

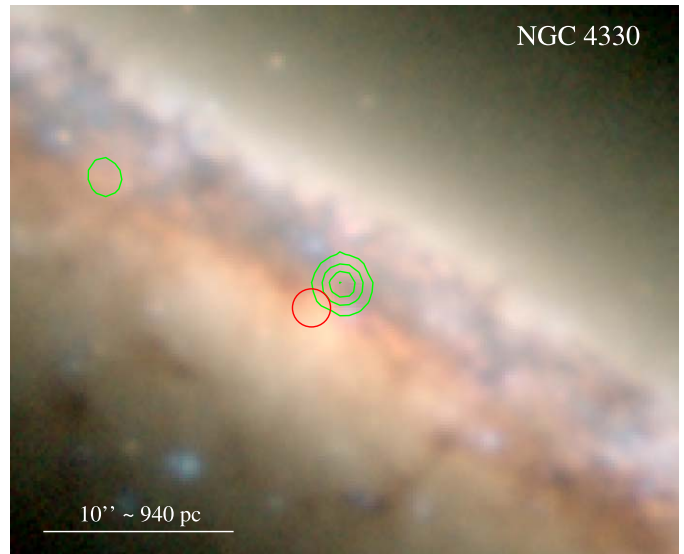
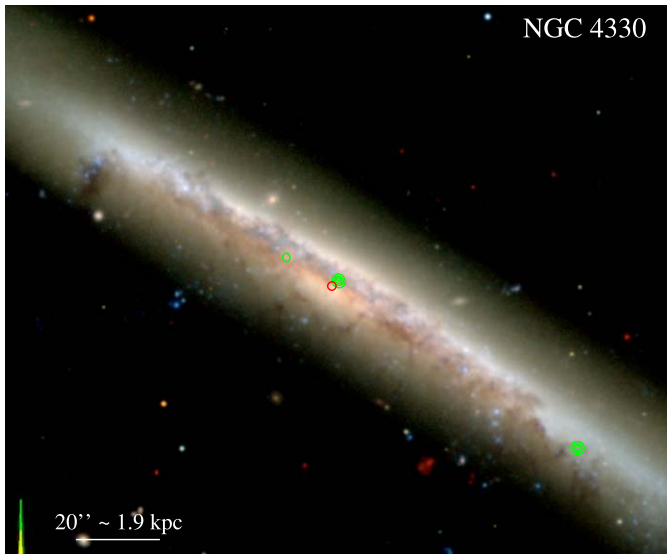


Figure 12. Similar to Figure 4, but displaying an NGVS image of NGC 4330.

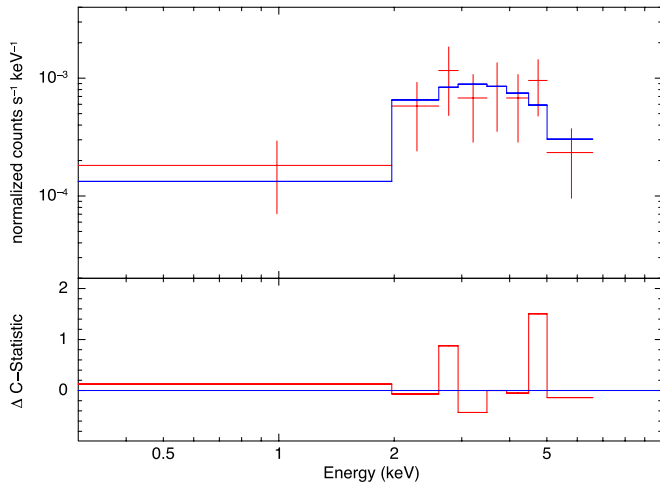


Figure 13. Similar to Figure 5, but for the edge-on galaxy NGC 4330, whose published optical center may be displaced due to the intervening dust.

central X-ray point source has only a few counts, they all have energies above 1 keV, which suggests that the $N_{\text{H,intrin}}$ absorption in NGC 4607 is quite high. The position of the source disfavors an XRB in the outskirts of this galaxy due to the required coincidence that it lines up with our sightline to the center of this galaxy. Moreover, Decarli et al. (2007) have reported that NGC 4607 is a known LINER.

We constructed the X-ray spectrum using the CIAO task *specextract*, before regrouping the spectra to 1 count per bin prior to the Cash statistics analysis in XSPEC using a fixed power-law slope $\Gamma = 1.7$ and a free $N_{\text{H,intrin}}$. The spectrum is shown in Figure 17. Although ratty, we wish to point out the grouping of counts around 6.4 keV. Although it could be due to the randomness of small number statistics, it is more likely due to a strong Fe K_{α} fluorescence line (and a Compton reflection bump above 10 keV) from cold, near-neutral, material (disk, torus, or clouds) irradiated by the nuclear X-ray source (Pounds et al. 1990). We hope to acquire a longer Chandra, or a new NuSTAR (Harrison et al. 2013), observation in the future, also enabling a better constraint on the slope of the X-ray SED.

4. Prospects for Black Hole Masses from the X-Ray Data

4.1. X-Ray Spectra

Longer CXO exposures, plus NuSTAR and XMM-Newton exposures—if its larger PSF does not encounter “crowding” issues and the source count is high enough to overcome the larger background level—would be of benefit. This would enable the X-ray SED modeling of the high-energy X-ray photons coming from hot accretion disks, and/or Compton scattering in a hot inflow, or inverse Compton emission from the magnetically powered jet base or corona above the disk, and/or synchrotron X-ray emission related to the unobscured part of an inner jet (e.g., Pringle & Rees 1972; Narayan & Yi 1995; Tzanavaris & Georgantopoulos 2007). Longer X-ray exposures would be valuable for establishing, through higher quality spectra, the existence of a possible dual AGN, similar to the X-ray pair in NGC 6240 (Komossa et al. 2003; Fabbiano et al. 2020).

Although it is not yet feasible with the available X-ray data to definitively distinguish between a stellar mass and an IMBH/AGN, we outline two possible spectral clues that can be pursued via deeper CXO observations and/or with the proposed next generation of X-ray satellites including Athena (Nandra et al. 2013; Rau et al. 2013), AXIS (Mushotzky 2018), and Lynx (Gaskin et al. 2019).

The first distinction we address is between stellar-mass black holes and IMBHs. Standard accretion-state models predict that an IMBH or AGN at a luminosity of $\sim 10^{38}$ – 10^{39} erg s^{-1} should have an unbroken power-law spectrum in the 0.5–10 keV band (low/hard state), while a stellar-mass source (especially a stellar-mass black hole) should have a disk-blackbody spectrum with a temperature ~ 0.5 –1 keV (high/soft state) and a normalization corresponding to characteristic radii ~ 50 –100 km. For example, this was the main argument in favor of the identification of the nuclear source in M33 (~ 20 times closer to us than the Virgo cluster) as a stellar-mass black hole (Foschini et al. 2004). There are, however, additional caveats in this simple classification. While transient stellar-mass black holes near their Eddington luminosities can exhibit hard power-law spectra in the hard intermediate state, these

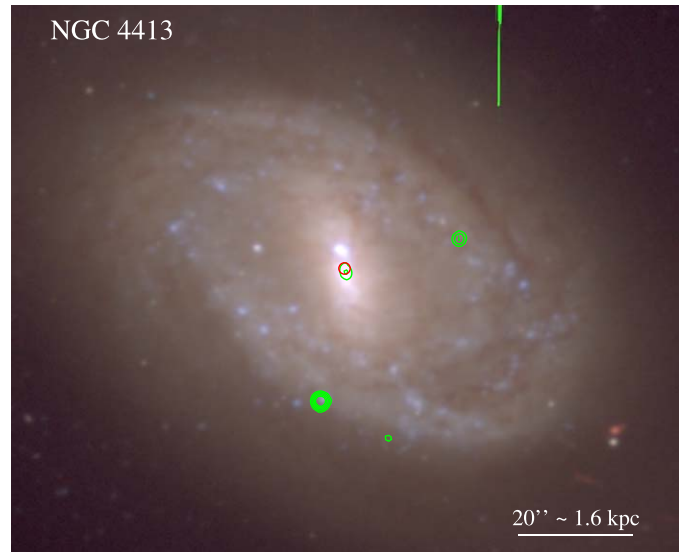
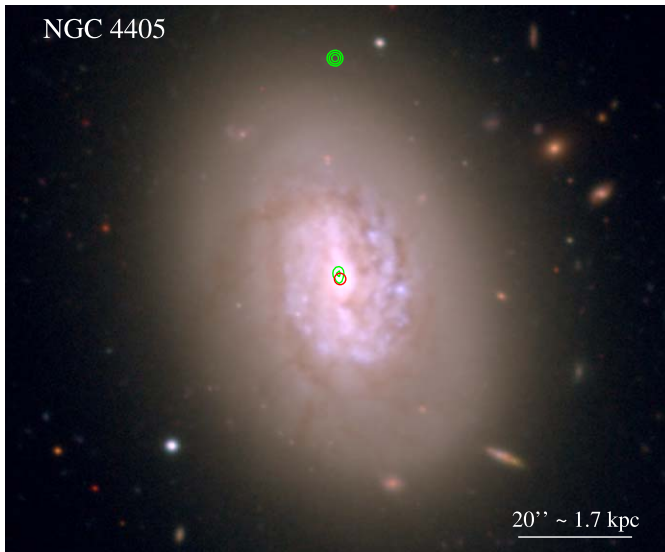


Figure 14. Similar to Figure 2, but displaying NGVS images of NGC 4405 and NGC 4413 (aka NGC 4407). For these two galaxies, the central X-ray photon count was low, and as such we tentatively consider them to be X-ray point sources.

phases are short-lived, typically lasting only a few days, and hence it is rather unlikely that a Chandra observation would catch a source in such a state (e.g., Homan & Belloni 2005; Motta et al. 2009). Moreover, neutron star X-ray binaries (X-ray pulsars) can also reach or exceed such luminosities, and at a moderate signal-to-noise ratio, the Comptonized spectrum of those sources is also well approximated by a hard power law, in the relatively narrow Chandra or XMM-Newton bands (Ferrigno et al. 2009; Farinelli et al. 2016; Pintore et al. 2017). The X-ray-to-optical flux ratio criterion is also inapplicable for nuclear sources, because in most cases we can only measure the optical brightness of the host star cluster, not the direct optical emission from the disk or the donor star of the X-ray source. As an indication of the difficulty of the task for galaxies in the Virgo cluster, one need only read the discussion about the nuclear black hole identification in the much closer M83 galaxy by Russell et al. (2020).

The second distinction, although likely an artificial one created out of observational selection bias, is between IMBHs (10^2 – $10^5 M_\odot$) and SMBHs in the 10^6 – $10^7 M_\odot$ mass range. In the X-ray luminosity range $\sim 10^{38}$ – 10^{39} erg s^{-1} , both an IMBH and a “normal” SMBH, with say $M_{\text{bh}} \sim 10^6 M_\odot$, would be lumped together in the low/hard state, according to the traditional state classification. However, more recent studies of accreting BHs in this low-luminosity regime show further physical changes as a function of the Eddington ratio $\equiv L_{\text{bol}}/L_{\text{Edd}}$ ($\approx L_X/L_{\text{Edd}}$ for stellar-mass BHs). The hardest spectra ($\Gamma \approx 1.7$) occur at an Eddington ratio of $\sim 10^{-3}$; below that threshold, the X-ray spectrum progressively softens again, reaching an asymptotic value of $\Gamma \approx 2.1$ at an Eddington ratio of $\sim 10^{-5}$ and below (Sobolewska et al. 2011; Armas Padilla et al. 2013; Plotkin et al. 2013; Yang et al. 2015; Plotkin et al. 2017). For example, an SMBH with M_{bh} around a few $10^6 M_\odot$ and $L_X \approx$ a few 10^{38} erg s^{-1} will have an Eddington ratio $\sim 10^{-5}$ (assuming a bolometric correction $L_{\text{bol}}/L_X \approx 10$; Lusso et al. 2012). Instead, an IMBH at the same X-ray luminosity may have an Eddington ratio of $\sim 10^{-3}$. Thus, a low-state IMBH should have a moderately harder spectrum than a more massive nuclear BH, at the same X-ray luminosity. We suggest that for a sufficiently high signal-to-noise ratio in the X-ray spectra, it will be possible to discriminate

between the two cases: if not for individual sources, at least based on the statistical distribution of fitted photon indices.

4.2. X-Ray Luminosities: the Fundamental Plane of Black Hole Activity

The “fundamental plane of black hole activity” for black holes with low accretion rates (Merloni et al. 2003; Falcke et al. 2004; Fischer et al. 2021) encompasses stellar-mass black hole X-ray binaries and AGN, and enables one to estimate the black hole mass based upon the nuclear radio emission, $L_R = \nu L_\nu$ erg s^{-1} (at 5 GHz), and the unabsorbed nuclear X-ray luminosity, L_X erg s^{-1} (at 0.5–10 keV). Although, it is noted that some AGN are X-ray luminous but radio silent (Radcliffe et al. 2021). Plotkin et al. (2012) report the following correlation for radio active systems:

$$\log L_X = (1.45 \pm 0.04) \log L_R - (0.88 \pm 0.06) \log M_{\text{bh}} - (6.07 \pm 1.10). \quad (5)$$

For $M_{\text{bh}} = 10^5 M_\odot$ and $L_X = 10^{40}$ erg s^{-1} , one obtains an expected radio luminosity $\nu L_\nu(5 \text{ GHz})$ of $10^{34.8}$ erg s^{-1} , while for $M_{\text{bh}} = 3 \times 10^3 M_\odot$ and $L_X = 10^{38}$ erg s^{-1} , one obtains an expected radio luminosity $\nu L_\nu(5 \text{ GHz})$ of $10^{32.5}$ erg s^{-1} . At an average distance of 17 Mpc, this corresponds to 0.04 mJy and 0.18 μJy , respectively. Using the correlation from Gültekin et al. (2019), which is based on the 2–10 keV luminosity³³, these estimates are 0.03 mJy and 0.08 μJy . This latter value is ~ 7 times smaller than the estimate of 0.54 μJy obtained using the earlier correlation from Gültekin et al. (2009).

For reference, Strader et al. (2012) searched for radio emission from potential IMBHs in three globular clusters but found no source down to rms noise levels of 1.5–2.1 $\mu\text{Jy beam}^{-1}$ with the Very Large Array (VLA). Tremou et al. (2018) have also reported a nondetection of IMBHs with $M_{\text{bh}} \gtrsim 10^3 M_\odot$ (3σ) in globular clusters, with a VLA image stack of 24 GCs having an rms sensitivity of 0.65 $\mu\text{Jy beam}^{-1}$, and an Australia Telescope Compact Array (ATCA) image stack of 14 GCs having an rms sensitivity of 1.42 $\mu\text{Jy beam}^{-1}$.

³³ For $\Gamma = 1.7$, $L_{2-10 \text{ keV}} = 0.646 L_{0.5-10 \text{ keV}}$.

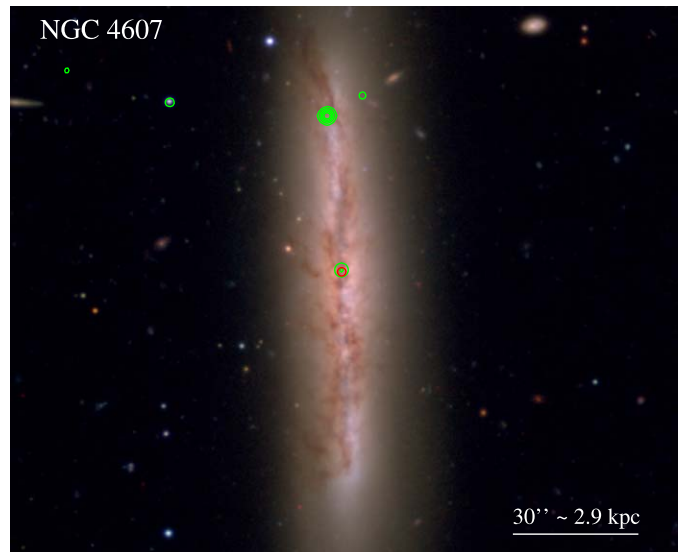
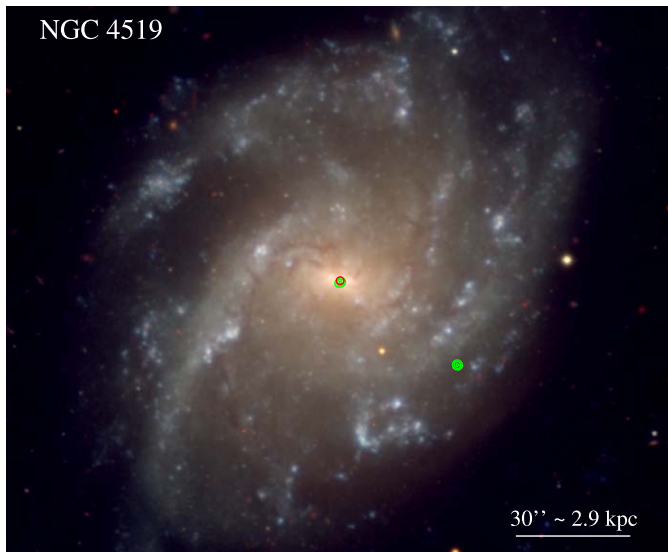
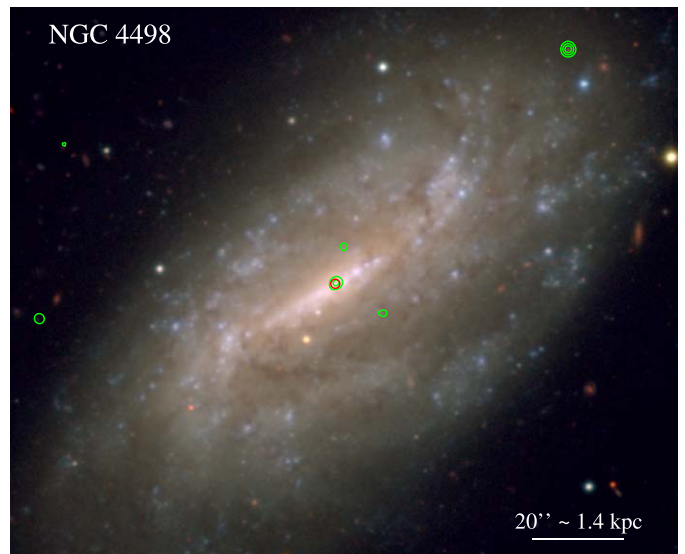
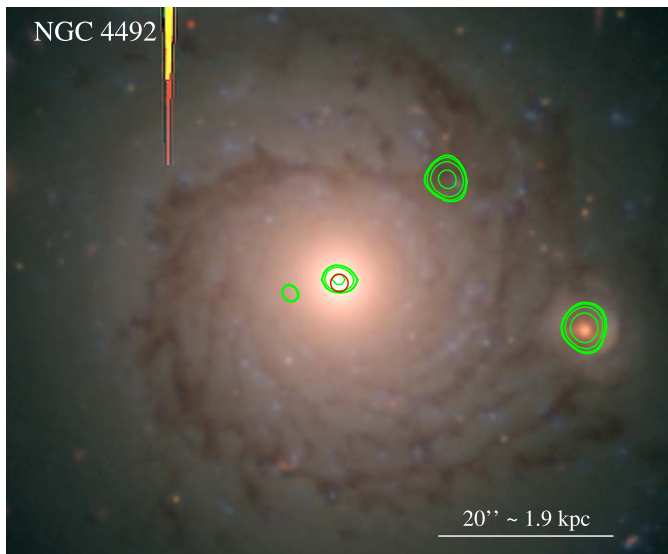


Figure 15. Similar to Figure 2, but displaying NGVS images of NGC 4498, NGC 4519, NGC 4492, and NGC 4607. For NGC 4492, the bright source to the right is the nucleus of the galaxy SDSS J123057.82+080434.7 (Wang et al. 2016), and the red/yellow “bleed” is from a bright adjacent star.

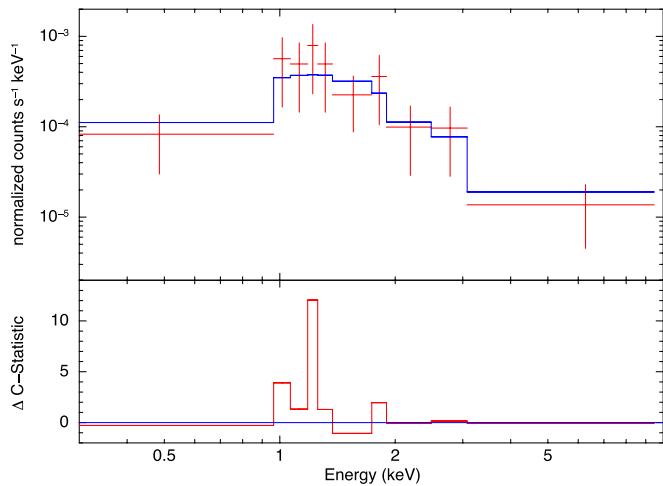


Figure 16. Similar to Figure 5, but for NGC 4492.

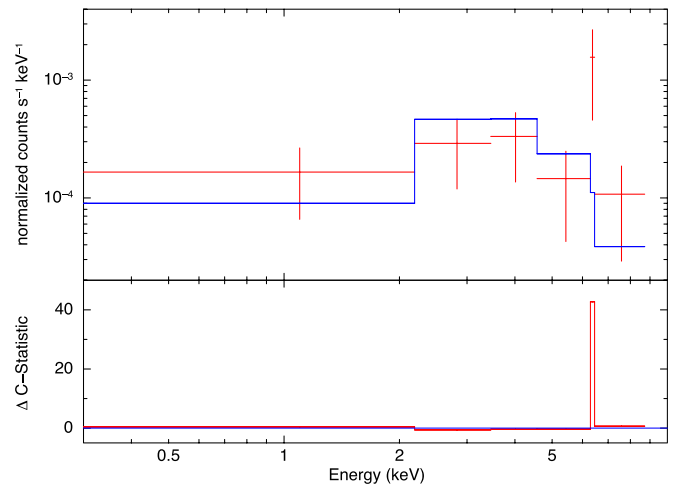


Figure 17. Similar to Figure 5, but for NGC 4607.

It will, however, be interesting to explore the Andromeda galaxy’s very low metallicity globular cluster RBC EXT8 (Larsen et al. 2020)—taken from the Revised Bologna Catalogue (Galleti et al. 2004)—which may have formed more massive stars than is usual, and might have formed an IMBH (Mapelli et al. 2021; see also Wan et al. 2020 in regard to the Phoenix GC and stream).

Reversing tact, one can use X-ray luminosities and radio observations to predict the black hole masses, or at least obtain an upper limit if only upper limits to the radio luminosity of potential compact nuclear sources are found. We scanned the literature for radio data from our sample, and found one observation. With $0''.15$ spatial resolution, Nagar et al. (2005) reported an upper limit to the nuclear flux in NGC 4713 of ≈ 1.10 mJy at 15 GHz (2 cm), or $\log(L_{\nu,15\text{ GHz}} \text{ W Hz}^{-1}) < 19.63$ for $D = 17.9$ Mpc. This equates to $\log(\nu L_{\nu,15\text{ GHz}} \text{ erg s}^{-1}) < 36.81$. However, we do not know the slope of the radio SED, required to obtain the luminosity at 5 GHz. Moreover, given the available X-ray flux and anticipated black hole mass in NGC 4713, one requires constraints on the radio flux which are some three orders of magnitude tighter, at around $1 \mu\text{Jy}$. Adding to the challenge, Nagar et al. (2005) report significant inter-year variability at 15 GHz and, for a given black hole, the radio and X-ray flux are correlated (Hannikainen et al. 1998; Brocksopp et al. 1999; Corbel et al. 2003), hence Equation (5).

Capetti et al. (2009) obtained VLA images for 63 of the 100 early-type galaxies in the Virgo cluster compiled by Côté et al. (2004), but they detected compact radio sources at the centers of just 12 of these (with fluxes from 0.13 mJy to 2.7 Jy), and no compact radio cores in any of the 30 lowest mass galaxies with $M_{*,\text{gal}} < 1.7 \times 10^{10} M_{\odot}$. In GSD19, we reported that only three of the 30 galaxies (from the larger set of 100) that were expected to have a central IMBH also had a central X-ray point source. However, for our sample of 75 spiral galaxies with ongoing star formation, and thus cold gas to potentially fuel a greater level of accretion onto a central IMBH, we have found that 13 of the 34 galaxies expected to have an IMBH (or 14 from 35 when including NGC 4212) also have an X-ray point source in their center. As such, there is hope for detecting the brighter sources in our sample at radio wavelengths, and the large collecting area of radio facilities with the spatial resolution to detect compact radio sources, such as the VLA, the next generation Very Large Array (ngVLA; Carilli et al. 2015), and the upcoming Square Kilometer Array radio telescope (SKA; Dewdney et al. 2009), will play a key role in detecting the fainter sources.

4.3. X-Ray Contamination: X-Ray Binaries

Here we consider the possibility that some of the nuclear X-ray point sources are XRBs, powered by an accreting neutron star or a $\sim 10 M_{\odot}$ black hole, rather than a massive black hole. Distinguishing between the two possibilities for individual sources can be difficult even at distances much closer than the Virgo cluster. A classic example of this situation is the bright ($L_X \approx 2 \times 10^{39} \text{ erg s}^{-1}$) point-like X-ray source in the nucleus of the Local Group’s late-type spiral galaxy M 33 (Dubus & Rutledge 2002), which is almost certainly a stellar-mass X-ray binary rather than an IMBH, based on its spectral and timing properties (Dubus et al. 2004; Middleton et al. 2011; La Parola et al. 2015; Krivonos et al. 2018). At the distance of the Virgo cluster, it would be impossible to tell.

Therefore, we need to assess the XRB contamination on a statistical level.

X-ray binaries are usually divided into two classes, based on the age and mass of their donor star. High-mass X-ray binaries (HMXBs) have a young donor, typically more massive than $\sim 10 M_{\odot}$. Since massive stars live for less than a few 10^7 yr, HMXBs are located in regions of current or recent star formation. As a first approximation, their number is linearly proportional to the star formation rate (Mineo et al. 2012; Lehmer et al. 2019). Low-mass X-ray binaries (LMXBs), instead, have a low-mass donor star, and ages $\gtrsim 10^9$ yr. Their number and spatial distribution in a galaxy approximately follow the stellar-mass distribution (Kim & Fabbiano 2004; Zhang et al. 2012). In more detail, their number is a function of the integrated star formation rate over the galaxy history (see Fragos et al. 2013). The LMXB population of a galaxy is itself composed of two subpopulations: one formed in globular clusters and the other in the field of the galaxy. Due to the higher stellar density and a higher rate of stellar encounters in globular clusters, they are ~ 1000 times more efficient than field stars at forming LMXBs, per unit stellar mass (Sivakoff et al. 2007; Kim et al. 2013; Lehmer et al. 2020). The HMXBs, on the other hand, are not known to get such a boost (Garofali et al. 2012; Johns Mulia et al. 2019); they are generally not formed from close encounters and captures like LMXBs, but instead come from the initial fragmentation of molecular clouds.

Spiral galaxies usually contain a mix of HMXB and LMXB populations. The HMXBs dominate for specific star formation rates $\log(\text{sSFR}) \gtrsim -10.5 \text{ yr}^{-1}$ (Lehmer et al. 2019). They also dominate the high-luminosity end of the distribution, at $L_X \gtrsim 10^{39} \text{ erg s}^{-1}$ (Lehmer et al. 2019). Soria et al. (2021) extensively report on the star formation rate, and off-center ULX population, among our parent sample of 75 Virgo cluster spiral galaxies. Our subsample in Table 1 has star formation rates ranging from 0.2 to $1.1 M_{\odot} \text{ yr}^{-1}$, with two galaxies having a rate of just $0.1 M_{\odot} \text{ yr}^{-1}$ (Boselli et al. 2015), and none of these galaxies appear to contain a nuclear starburst. This corresponds to specific star formation rates $\log(\text{sSFR yr}^{-1})$ ranging from -9.6 to -10.5 , with the two low star formation rate galaxies having logarithmic specific star formation rates of -11.0 and -11.5 . While these latter two galaxies are expected to have more LMXBs than HMXBs brighter than $L_{0.5-8\text{ keV}} = 10^{38} \text{ erg s}^{-1}$, this reverses for the galaxies with higher specific star formation rates. For a rate of -10.5 , one expects three HMXBs brighter than $10^{38} \text{ erg s}^{-1}$ and one brighter than $6 \times 10^{38} \text{ erg s}^{-1}$. For a specific star formation rate of -9.6 , one expects eight HMXBs brighter than $10^{38} \text{ erg s}^{-1}$ and three brighter than $6 \times 10^{38} \text{ erg s}^{-1}$. However, the star formation rates reported above are for the whole galaxy, including their spiral arms. For the galaxies in our subsample, the rates in the nuclear regions alone (within 100 parsec of the nuclear position) are roughly 3 to 4 orders of magnitude lower. That is, around $\log(\text{sSFR yr}^{-1}) \approx -12.5$ or lower. Therefore, the probability of finding an HMXB at the nuclear position is low.

The second possibility of contamination is from field LMXBs, in galaxies where the stellar mass in the nuclear region is dominated by field stars rather than a nuclear star cluster. For a stellar mass³⁴ of $10^{10} M_{\odot}$, we expect ~ 5 LMXBs more luminous than $10^{38} \text{ erg s}^{-1}$, and ~ 1 LMXB more luminous than $5 \times 10^{38} \text{ erg s}^{-1}$ (those numbers are a few times

³⁴ Our subsample of spiral galaxies with candidate IMBHs have stellar masses $(0.3-10) \times 10^{10} M_{\odot}$ (GSD19).

lower in elliptical galaxies because their stellar population is older). The question then becomes how much of that stellar mass is within the inner region. For a disk with a typical exponential scalelength, h , of 3 kpc (e.g., Graham & Worley 2008), the half-light radius $R_c = 1.678 \times 3 \approx 5$ kpc. Using the equations from Graham & Driver (2005), the fraction of light within the inner 80 pc ($\approx 1''$) radius is 3.5×10^{-4} , and within the inner 160 pc ($\approx 2''$) radius it is 1.4×10^{-3} . Therefore, the probability of a field-LMXB located at the nuclear position is also small. To give a specific example, one would expect $3.5 \times 10^{-4} \times 5 \approx 0.002$ LMXBs more luminous than 10^{38} erg s $^{-1}$ within the inner 80 pc ($\approx 1''$) radius of a spiral galaxy with a stellar mass of $10^{10} M_\odot$. That is, just 1-in-50 will be expected to have such an LMXB.

Finally, we consider the possibility of finding a bright LMXB inside a nuclear star cluster. For this case, we already know that the probability is not negligible, as the example of M33 shows. To estimate this, we assume that a nuclear star cluster is equivalent to a GC of similar mass, and examine the number of LMXBs observed in the latter class of systems. From a study of GCs around Virgo and Fornax elliptical galaxies, Kim et al. (2013) found that about 5% of red GCs, and about 1.5% of blue GCs, contain an LMXB more luminous than 10^{38} erg s $^{-1}$ at 0.3–8 keV. This drops to 2.7% (red) and 0.8% (blue) for $L_{0.3-8 \text{ keV}} \geq 2 \times 10^{38}$ erg s $^{-1}$. Considering only GCs more luminous than $M_z \approx -10$ mag (a better comparison for our nuclear star clusters, which have masses from $0.5 \times 10^6 - 2 \times 10^7 M_\odot$),³⁵ Kim et al. (2013) showed that the bright LMXB occupation fraction was higher by a factor of 3, for both red and blue GCs. This is consistent with the results of Sivakoff et al. (2007), who also found an occupation fraction of $\sim 10\%$ – 20% for LMXBs above 10^{38} erg s $^{-1}$ in the most massive red GCs, and a factor of 3 lower in the most massive blue GCs. In our sample of Virgo spiral galaxies expected to host an IMBH, we found an X-ray point source occupation fraction of 12-from-33, or 14-from-35, which is roughly 36% or 40%.

Moreover, the above percentage of 36% represents a lower limit to the true value of spiral galaxies having central sources with $L_X > 10^{38}$ erg s $^{-1}$ because our data was usually not deep enough to detect X-ray sources as faint as 10^{38} erg s $^{-1}$, even under the assumption of no intrinsic neutral gas absorption. For sources not significantly affected by intrinsic absorption (e.g., at the outskirts of a galactic disk or in regions dominated by old stellar populations), our CXO data, with typical exposure times of ~ 10 ks, has a detection limit around $3-4 \times 10^{38}$ erg s $^{-1}$ (Soria et al. 2021). For comparison, the early-type galaxy sample was observed to a similar depth of 3.7×10^{38} erg s $^{-1}$ (Gallo et al. 2010). Only a few large galaxies in our sample have longer archival observations that enabled us to reach detection limits around 10^{38} erg s $^{-1}$.

Furthermore, we do know that late-type galaxies have generally more X-ray-absorbing cold gas in their nuclear regions than early-type galaxies (in which the gas is mostly ionized). For disk galaxies seen at a high inclination, the absorbing column density through the disk plane also has to be added to the intrinsic absorption in the nuclear region. For plausible HI column densities of $\approx 3 \times 10^{22}$ (100 times the Galactic line-of-sight value in the Virgo direction, corresponding to about 15 mag of extinction in the V band), the detection limit at 17 Mpc in a typical

10-ks observation is reduced to $\approx 10^{39}$ erg s $^{-1}$. Sources with luminosities of a few 10^{38} erg s $^{-1}$ are much more likely to be detected in the nuclear region of early-type Virgo galaxies than disk galaxies. Thus, we argue that if we could remove the effect of the obscuring HI gas, the 36% detection rate would rise while the 10% figure for the early-type galaxies would not change.

The above value of 36% is 3.6 times higher than the ratio of 3-from-30 (10%) found by Graham & Soria (2019) among the Virgo cluster dwarf early-type galaxies expected to have an IMBH and similarly imaged through a CXO Large Project with long exposure times. The explanation may be that the more gas-rich environment of the star-forming, late-type spiral galaxies is more favorable for igniting the central black hole and turning on an AGN than the environment within the dwarf early-type galaxies (Kauffmann & Heckman 2009). Collectively, the findings above may be suggesting that we are not just detecting XRBs involving a donor star feeding the accretion disk around a compact stellar-mass black hole or neutron star (e.g., Casares et al. 1992; Soria & Wu 2003; Casares et al. 2014). One could spend an inordinate amount of energy and text trying to refine the negligible probabilities of detecting a field-XRB within the inner arcsecond or two of each galaxy, including considerations of the (host galaxy's) stellar mass, star formation rate, and metallicity within the region sampled by CXO. Ultimately, all that effort would be undermined because there would need to be a recognition that we do not yet know with certainty how many XRBs are expected for a given nuclear star cluster (mass, metallicity, and star formation rate)³⁶, and their XRB contribution is expected to dominate over the field population given the findings in globular clusters. However, there is already a clincher against a population of solely XRBs. We already know that four³⁷ of our late-type galaxies are LINERs, and NGC 4178 has a high-ionization [Ne V] emission line (Satyapal et al. 2009), likely flagging the existence of a massive black hole. Nonetheless, it remains desirable to know what the prospects are for constraining the masses of these suspected IMBHs. In what follows, we provide a concerted and substantial discussion for where and how further progress on this front can be made through recourse to non-X-ray data.

5. Prospects for Black Hole Masses from Non-X-Ray Data

In what follows, we review the prospects for spatially resolving the sphere of gravitational influence around IMBHs. This offers the promise of direct mass measurement. We further discuss additional prospects, involving non-X-ray data, for determining the presence and mass of IMBHs.

5.1. Chasing the Sphere of Influence

From our parent sample of 74+1 late-type galaxies in the Virgo cluster, only three (NGC 4303, NGC 4388, and NGC 4501)³⁸ have had directly measured black hole masses reported (see Table A2 in GSD19). That is, their black hole's sphere of

³⁵ These masses are typical for star clusters (Scott & Graham 2013), and they are similar to the nuclear star cluster masses in the 30 early-type galaxies predicted to harbor an IMBH by Graham & Soria (2019).

³⁶ The pursuit of nuclear star cluster metallicities, stellar ages, and star formation rates is well beyond the scope of the current investigation.

³⁷ NGC 4713 and NGC 4212 are LINER/H II composites, NGC 4313 is a Seyfert/LINER and NGC 4607 is a LINER.

³⁸ The recent compilation of directly measured black hole masses given by Sahu et al. (2019b) reports two additional late-type galaxies with directly measured black hole masses in/near the Virgo cluster. They are NGC 4151 (Gursky et al. 1971; Wood et al. 1984) with $M_{\text{bh}} \sim 5 \times 10^7 M_\odot$, and NGC 4699 (González Delgado et al. 1997) which belongs to the NGC 4697 Group (Makarov & Karachentsev 2011) and has $M_{\text{bh}} \sim 2 \times 10^8 M_\odot$.

Table 3
Black Hole Calibration Points

M_{bh} M_{\odot}	σ km s ⁻¹	r_{soi} pc (")
10 ⁹	293	50 (0.6)
10 ⁸	195	11.3 (0.14)
10 ⁷	130	2.5 (0.03)
10 ⁶	86	0.6 (0.007)
10 ⁵	57	0.13 (1.6E-3)
10 ⁴	38	0.03 (3.6E-4)
10 ³	25	0.007 (8.3E-5)
10 ²	17	0.001 (1.8E-5)

Note. Reversing the spiral galaxy $M_{\text{bh}}-\sigma$ bisector relation (Davis et al. 2017, Table 4 entry “All”) we provide both the stellar velocity dispersion that corresponds to the black hole masses listed in column 1 and the expected sphere of influence (soi) of the black hole if at a typical Virgo cluster distance of 17 Mpc.

influence should have been spatially resolved. While two of these are reported to have black hole masses greater than $\sim 10^7 M_{\odot}$, NGC 4303 ($D \approx 12\text{--}13$ Mpc, $\sigma = 95$ km s⁻¹) has the smallest reported black hole mass of the three, at $4 \times 10^6 M_{\odot}$ (Pastorini et al. 2007, observed with HST/STIS). For reference, from the sibling sample of 100 early-type galaxies in the Virgo cluster (Côté et al. 2004) that were also observed with CXO (Gallo et al. 2008), there are 11 galaxies that have directly measured black hole masses (see Table 1 in Graham & Soria 2019), and all but one of those³⁹ have black hole masses greater than $\sim 2 \times 10^7 M_{\odot}$.

Table 3 reveals the typical spatial resolution required to resolve the gravitational sphere of influence (soi) around black holes of different mass and located at a typical Virgo cluster distance of 17 Mpc. These estimates are based upon the expression $r_{\text{soi}} = GM_{\text{bh}}/\sigma^2$ (Peebles 1972; Frank & Rees 1976), which is informatively reviewed in Merritt & Ferrarese (2001) and Merritt (2013), and the spiral galaxy $M_{\text{bh}}-\sigma$ relation from Davis et al. (2017). Obviously for local galaxies, if they are half this assumed distance then their apparent r_{soi} (in arcseconds, not in parsecs) will double.

It is pertinent to ask, and interesting to know, what prospects there are for high(er) spatial resolution observations than used thus far. In space, the 6.5 m James Webb Space Telescope (JWST) will hopefully soon accompany the 2.4 m HST, with NIRCam (Horner & Rieke 2004) aboard JWST providing a diffraction-limited spatial resolution of ≈ 70 mas, as defined by the PSF’s FWHM at 2 microns. This is comparable to the angular resolution achieved at UV wavelengths with HST’s long-slit Space Telescope Imaging Spectrograph (STIS; Woodgate et al. 1998). The upcoming 24.5 m Giant Magellan Telescope (GMT) is expected to have a diffraction-limited resolution of ~ 13 mas in the Jband (~ 22 mas in the Kband) feeding the GMT integral field spectrograph (GMTIFS; McGregor et al. 2012), while the Thirty Meter Telescope (TMT) boasts 4 mas spaxels and 8 mas resolution from its Infrared Imaging Spectrograph (IRIS; Larkin et al. 2016). The 40 m Extremely Large Telescope (ELT) will be equipped with

³⁹ NGC 4486A (VCC 1327, $D = 18.3$ Mpc, $\sigma = 131 \pm 13$ km s⁻¹) has the lowest reported black hole mass of the 11 early-type galaxies at $(1.3 \pm 0.8) \times 10^7 M_{\odot}$. It was observed with the integral field spectrograph SINFONI on the Very Large Telescope under 0.1" spatial resolution by Nowak et al. (2007).

the High Angular Resolution Monolithic Optical and Near-Infrared (HARMONI; Thatte et al. 2016) integral field spectrograph, also with 4×4 mas spaxels. This represents roughly an order of magnitude improvement, and will enable one to resolve the sphere of influence around Virgo cluster BHs of mass down to $10^6 M_{\odot}$ (see Table 3). For the 100+ galaxies within the Local Group that are more than ten times closer than the Virgo cluster’s mean distance, i.e., within 1.7 Mpc, the TMT and ELT will be able to probe BHs that are some ten times smaller, encompassing the galaxies M33, NGC 185, NGC 205, NGC 300, NGC 147, NGC 3109, NGC 6822, IC 10, IC 1613, IC 5152, UGC 4879, DDO 216, DDO 210, DDO 221, Leo I, II and III, Sextans A and B, Antlia, etc. One will even be able to probe down to black hole masses of $10^4 M_{\odot}$ if they are within 170 kpc, encompassing the many satellites of the Milky Way, such as the Magellanic Clouds located 50 and 63 kpc away, Sextans, Ursa Minor, Draco, Fornax, Sculptor, Carina, Pisces I, Crater II, Antlia 2, etc. Although, for BHs with a mass of $10^4 M_{\odot}$ and a sphere of influence equal to 0.03 pc (based on a host system stellar has a velocity dispersion of 38 km s⁻¹), the number of stars within the sphere of influence may be limited. Excitingly, the sphere of influence around possible IMBHs within the Galaxy (see Oka et al. 2017; Ravi et al. 2018), out to distances of 17 kpc, could be resolvable for masses down to $10^3 M_{\odot}$.

Impressively, the GRAVITY near-IR (Kband) interferometric instrument involving all four of the 8 m Very Large Telescopes (VLT) already provides 4 mas resolution, or 2 mas resolution if using the four 1.8 m Auxiliary Telescopes (e.g., GRAVITY Collaboration et al. 2021). The planned optical interferometer for the VLT, MAVIS, will have a milliarcsecond spatial resolution at 550 nm (McDermid et al. 2020; Monty et al. 2021).

Considering facilities with longer baselines, ALMA, with its 16 km baseline, already provides 20 mas resolution at 230 GHz (1.3 mm), several times better than most current optical/near-IR telescopes. Radio observations by Miyoshi et al. (1995) of maser emission from a circumnuclear disk in NGC 4258 (M106) were made using a synthesized beam size of just 0.6×0.3 mas, obtained using 22 GHz (1.3 cm) interferometry on the Very Long Baseline Array (VLBA).⁴⁰ Indeed, this enabled confirmation that BHs are real, as opposed to say a swarm of compact stellar-mass remnants. Not surprisingly, this result led to searches for more such maser detections around BHs, and quite a few discoveries were made (e.g., Greenhill et al. 2003; Kuo et al. 2011; Humphreys et al. 2016). Most dramatically, recent observations at 1.3 mm wavelengths taken with the Event Horizon Telescope (EHT) have provided the highest resolution images to date. With 20 μas resolution, The Event Horizon Telescope Collaboration et al. (2019) probed not just within the sphere of influence, but were able to see the silhouette of the event horizon around the SMBH in M87, located ~ 17 Mpc away in the Virgo cluster. Such spatial resolution matches the sphere of influence that a 100 solar mass black hole would have 17 Mpc away (see Table 3), although the radio flux from such a source may not be high enough for the EHT (Fish et al. 2016). The Spektr-M mission (aka the Millimetron Space Observatory, launch date ~ 2030) will place a 10 m dish 1.5 million kilometers from Earth. It will operate at

⁴⁰ The VLBA can now achieve 0.12 mas (120 μas) resolution at a wavelength of 3 mm, using the MK-NL baseline, and the ngVLA may spatially resolve SMBH binaries and triples (Burke-Spolaor et al. 2018).

wavelengths from 0.07 to 10 mm. When joining the Earth-based interferometers, it will provide a 150 fold increase in spatial resolution, heralding in a new era of astronomy, with nanoarcsecond spatial resolution around 130 mas.

5.2. Potential Future Observations

There are several follow-up observations and investigations which would yield greater information and insight.

The large collecting area of the upcoming ngVLA and SKA, plus the Five-hundred-meter Aperture Spherical radio Telescope (FAST, aka Tianyan; Nan 2006; Li et al. 2013), and the current SKA pathfinder MeerKAT (originally the Karoo Array Telescope; Booth et al. 2009; Jonas 2009), and the Low-Frequency Array (LOFAR; van Haarlem et al. 2013) should prove valuable for detecting faint radio sources. Coupled with the improved spatial resolution from long-baseline interferometry, one could search for masers around IMBHs (e.g., Green et al. 2015) and probe the immediate vicinity of the AGN and the base of their jets (Tingay et al. 2000; Hough et al. 2002; Paragi et al. 2015; Doi et al. 2013; Janssen et al. 2021). As noted before, the radio luminosities can also be combined with the X-ray luminosity for use in the “fundamental plane of black hole activity” (Merloni et al. 2003; Falcke et al. 2004; Dong & Wu 2015; Liu et al. 2016; Nisbet & Best 2016) to estimate the mass of the black hole (Section 4.2).

Reverberation mapping of AGN can probe the gas clouds within the BH’s sphere of influence, although the assumptions about the orbital stability (virialized nature) and geometry of these clouds, coupled with the use of a mean virial f -factor to convert virial products, $r\Delta V^2/G$, into virial masses (e.g., Bahcall et al. 1972; Peterson & Wandel 2000), can hinder confidence in the estimated black hole mass. In application, the virial factor is currently assumed to be constant for all AGN, and for IMBHs it is further based upon the assumption that this constant value can be extrapolated to masses less than $\sim 10^6 M_\odot$, i.e., below masses used to establish its value (e.g., Peterson et al. 2004; Graham et al. 2011). The characteristic timescale at which the power spectrum of a galaxy’s central optical continuum variability flattens has also been shown to scale with black hole mass (Burke et al. 2021). When the Eddington ratio is sufficiently high, so that the variable optical continuum emission from the accretion disk (e.g., Sarajedini et al. 2003, 2006; Baldassare et al. 2018) is not swamped by the photon shot noise of the starlight in one’s aperture, this will provide yet another window of investigation. The upcoming, large-scale time-domain surveys such as LSST will be very useful in this regard (e.g., Choi et al. 2014; Ivezić et al. 2014).

Thanks to facilities like the Wide-field Infrared Survey Explorer (WISE; Wright et al. 2010) and the Spitzer Space Telescope (Werner et al. 2004), one can use mid-IR diagnostics to separate AGN from star formation. The presence of mid-IR high-ionization lines, combined with the strength of polycyclic aromatic hydrocarbon (PAH) emission features, can provide a means to discriminate between the dominant energy source within one’s aperture (e.g., Dale et al. 2006; Satyapal et al. 2009; Stern et al. 2012; Yao et al. 2020). The presence of high-ionization optical emission lines can also support the presence of a black hole (Baldwin et al. 1981; Veilleux & Osterbrock 1987; Kewley et al. 2006; Martínez-Palomera et al. 2020; Mezcua & Domínguez Sánchez 2020). Furthermore, the existence of Doppler-broadened emission lines—used in calculating the virial product under the assumption that the broadening traces

the velocity dispersion due to virialized motions around the black hole, as opposed to non-virialized motion or outflows (e.g., Manzano-King et al. 2019, Appendix A)—can be used to infer the presence of an IMBH rather than a stellar-mass black hole (Baldassare et al. 2015; Chilingarian et al. 2018). We therefore intend to pursue the acquisition of Keck spectra to search for such optical emission lines in the Virgo cluster galaxies, enabling us to potentially derive a virial mass for the X-ray detected black holes.

The Kamioka Gravitational Wave Detector (KAGRA; Aso et al. 2013), with its 3 km baseline, and the famous LIGO/VIRGO facilities (Abramovici et al. 1992; Caron et al. 1997; Harry & LIGO Scientific Collaboration 2010; Acernese et al. 2015), are constrained to detect the collision of BHs less massive than $\sim 200 M_\odot$. Thus far, LIGO/VIRGO have reported a bounty of BHs with masses tens of times the mass of our Sun, along with the collisional-creation of a black hole with a mass equal to $98^{+17}_{-11} M_\odot$ (Zackay et al. 2021) and $142^{+28}_{-16} M_\odot$ (The LIGO Scientific Collaboration et al. 2020). The proposed underground Einstein Telescope (ET; Punturo et al. 2010; Gair et al. 2011; Huerta & Gair 2011) is planning to have a 10 km baseline with detector sensitivities that should enable it to detect IMBHs across the Universe, as will the planned Cosmic Explorer (CE; Reitze et al. 2019) with its 40 km baseline. It is anticipated that the planned space-based DECi-hertz Interferometer Gravitational wave Observatory (DECIGO; Kawamura et al. 2011; Ishikawa et al. 2021), and the European Laser Interferometer Space Antenna (LISA) (Danzmann & LISA Study Team 1997) will also help to fill the relative void between $\sim 10^2$ and $\sim 10^5 M_\odot$. They will be capable of capturing oscillations in the fabric of spacetime due to extreme- and intermediate-mass ratio inspiral (EMRI and IMRI) events around IMBHs (Gair et al. 2004; Mapelli et al. 2012; Merritt 2015; Babak et al. 2017; Bonetti & Sesana 2020), and IMBH-IMBH mergers from dwarf galaxy collisions (Bekki & Chiba 2008; Graham et al. 2012; Yozin & Bekki 2012; Cloet-Osselaer et al. 2014; Paudel et al. 2018; Barausse & Lapi 2020; Conselice et al. 2020; Zhang et al. 2020).

As seen here, it is known to be common for the centers of galaxies to house a nuclear star cluster (Reaves 1983; Binggeli et al. 1985; Sandage et al. 1985; Carollo et al. 1997; Matthews et al. 1999; Böker et al. 2002), including late-type galaxies and the dwarf early-type galaxies of the Virgo cluster (Ferrarese et al. 2006; Côté et al. 2006). Nuclear star clusters can reside in a more gas-rich environment than globular clusters because the gas escape speed, due to the surrounding galaxy, is higher than in globular clusters. Not surprisingly, such galaxy centers are suspected to be ripe fields for cataclysmic disruptions and mergers of stars, neutron stars, and black holes (e.g., Dokuchaev & Ozernoi 1981; Illarionov & Romanova 1988; Quinlan & Shapiro 1990; Pfister et al. 2020). They may also be the sites for some of the hard to spatially constrain gravitational waves arising from the collision of compact massive objects (Abbott et al. 2016a, 2016b; Andreoni et al. 2017; Abbott et al. 2018; Coughlin et al. 2019; The LIGO Scientific Collaboration et al. 2020), and the ejection site of high-velocity stars (e.g., Baumgardt et al. 2004; Levin 2006; Sesana et al. 2006; Kozlov et al. 2020). As done here, the stellar mass of the nuclear star cluster can be used to predict the resident black hole mass. This can be combined with multiple black hole mass estimates from a wide array of independent black hole mass scaling relations. Such an approach was used on the spiral

galaxy NGC 3319, which has a centrally located X-ray point source, and which initially had a black hole mass estimate of $3 \times 10^2 - 3 \times 10^5 M_\odot$ based on an assumed Eddington ratio of 0.001–1 (Jiang et al. 2018), but for whom an error-weighted meta-analysis of nine independent estimates of the black hole mass yielded $M_{\text{bh}} = (2.3_{-1.6}^{+5.3}) \times 10^4 M_\odot$ (Davis & Graham 2021).

6. Potential Dual and Off-center AGN

Normally, off-centered X-ray point sources are associated with XRBs. Indeed, the majority of off-centered ULXs have been found to be consistent with super-Eddington, stellar-mass accretors (Feng & Soria 2011; Kaaret et al. 2017). However, the current investigation suggests that some IMBHs may have X-ray luminosities of $10^{38} - 10^{40} \text{ erg s}^{-1}$, and thus comparable Eddington ratios (L_X/L_{Edd} , with $L_{\text{Edd}} = 1.3 \times 10^{38} M_{\text{bh}}/M_\odot \text{ erg s}^{-1}$) to many SMBHs. It is therefore conceivable, if not inevitable, that some off-centered X-ray point sources with $L_X = 10^{38} - 10^{40} \text{ erg s}^{-1}$ will be IMBHs.

The destructive creative process of galaxy evolution can see galaxies stripped to their nuclear core (e.g., Bekki et al. 2003; Graham 2020, and references therein), only to then merge and become part of a larger galaxy than they ever were (e.g., Tremaine et al. 1975; Graham et al. 2021, and references therein). This path, and no doubt others, is expected to yield galaxies with off-centered massive black holes, an informative clue to the growth of galaxies. In Section 3, we identified four galaxies with an additional, near-central X-ray point source. While these may well be XRBs, it is possible that they may be IMBHs.

Pairs of active BHs with large, kpc-sized offsets have regularly been reported in the literature. They are typically associated with close pairs of galaxies, perhaps a parent plus a satellite galaxy, and with the early stages of mergers (Bianchi et al. 2008; Comerford et al. 2009a; Civano et al. 2010; Fu et al. 2011; Comerford et al. 2015; Barrows et al. 2016, 2019; Rubinur et al. 2021; Li et al. 2021; Tubín et al. 2021; Kosec et al. 2017). After a significant galaxy accretion or merger event, the inspiral of the two massive black holes can result in dual AGN—if both black holes are active—with at least one black hole that is offset from the merged-galaxy center (Ballo et al. 2004; Guainazzi et al. 2005; Tremmel et al. 2018; Li et al. 2020).

NGC 6240 is one such galaxy with a dual X-ray AGN having a separation of ~ 1 kpc (Komossa et al. 2003; Fabbiano et al. 2020). CXO J101527.2+625911, with its spatial offset of 1.26 ± 0.05 kpc from its host galaxy’s center, has additionally been shown to have a velocity offset of $175 \pm 25 \text{ km s}^{-1}$ from the host galaxy (Kim et al. 2017). Dual black holes with subkiloparsec separation are also known (e.g., McGurk et al. 2015). In the radio galaxy 0402+379, Rodríguez et al. (2006) found a binary SMBH in the form of a spatially resolved, double radio-emitting nucleus with just a 7 pc separation (see also Burke-Spolaor 2011). Furthermore, many spectroscopic binaries, or at least systems with double-peaked emission lines, are known (Peterson et al. 1987; Zhou et al. 2004; Comerford et al. 2009b; Komossa et al. 2021), and the cyclical brightnesses of quasar PSO J185 is suggestive of a binary SMBH at subparsec separation (Liu et al. 2019).

The dual X-ray point source in NGC 4212, separated by ~ 240 pc (Figure 6), may be signaling the presence of a dual AGN, although unlike with the post-merger, late-type Virgo

cluster galaxy NGC 4424 (Graham et al. 2021)—which appears to show an off-centered infalling nuclear star cluster with an X-ray point source—there is no obvious evidence in the optical image for a recent merger (Morales et al. 2018). While the X-ray emission from the very center of NGC 4212 would tend to favor an association with the expected massive black hole, the nature of the nearby slightly off-center companion X-ray point source is less certain. Rather than being accreted, it may have formed in situ within, say, a star-forming clump (Pestoni et al. 2021). The same can be said about NGC 4313, whose two inner X-ray point sources are roughly twice as far apart as the pair in NGC 4212. While multiple black hole scaling relations predict the existence of a central $10^5 - 10^6 M_\odot$ black hole in NGC 4212, and we have found an X-ray point source coincident with the galaxy center, in regard to the off-center X-ray point source in this galaxy, there is the likely possibility of an XRB associated with a compact stellar-mass object (e.g., Feng & Soria 2011; Kaaret et al. 2017), or a distant AGN (e.g., Sutton et al. 2015).

The eventual coalescence of binary black holes may result in a gravitational wave recoil of the merged black holes, again resulting in an off-center position for the new larger black hole (Merritt et al. 2004; Merritt & Milosavljević 2005; Baker et al. 2006; Campanelli et al. 2007; Herrmann et al. 2007; Blecha & Loeb 2008; Komossa & Merritt 2008; Sundararajan et al. 2010; Blecha et al. 2016; Shen et al. 2019). Such recoils might take the surrounding star cluster with them (e.g., Merritt et al. 2009).

Offsets of $10 - 10^2$ parsecs from the optical centers of galaxies, as defined by their outer isophotes, have been observed among the dense $\approx 10^{6 \pm 1} M_\odot$ nuclear star clusters in low-mass Virgo cluster galaxies (Binggeli et al. 2000; Barazza et al. 2003). For reference, $1''$ at 17 Mpc is 82 parsecs. This offset is likely due, in part, to the shallow gravitational potential well of these low-Sérsic index galaxies (Davies et al. 1988; Young & Currie 1994; Jerjen et al. 2000; Terzić & Graham 2005), which can result in oscillations or wandering of the cluster about the galaxy center. The association of massive black holes with these nuclear star clusters has been known for over a decade (Graham & Driver 2007; González Delgado et al. 2008; Seth et al. 2008; Graham & Spitler 2009), and it has long been known that the two entities coexisted in the Milky Way (Lynden-Bell 1969; Sanders & Lowinger 1972; Rubin 1974) and M32 (Smith 1935; Burbidge 1970; Tonry 1984). Therefore, similar offsets between some AGN X-ray point sources and the optical center of the parent galaxy are to be expected, and have been found in low-mass galaxies (Mezcua & Domínguez Sánchez 2020). Indeed, even in some large galaxies, massive AGN have been found slightly (~ 10 pc) off-center (e.g., Batcheldor et al. 2010; Lena et al. 2014; Menezes et al. 2014), but more so in dwarf galaxies (Mezcua & Domínguez Sánchez 2020; Reines et al. 2020) and simulations of dwarf galaxies (e.g., Bellovary et al. 2019; Pfister et al. 2019). This is also to be expected if the dynamical friction timescale correlates inversely with the black hole mass.

7. Summary

As detailed above, there is a wealth of opportunity to further pursue the IMBH candidates identified here and those expected to reside in other low-mass galaxies. This is possible through longer X-ray exposures, simultaneous and deep radio observations, high signal-to-noise optical spectra, new mid-IR

diagnostic tools, plus a wealth of emerging facilities with higher spatial resolution, and gravitational wave detectors.

We have discovered central, or close to central, X-ray point sources in eleven Virgo cluster spiral galaxies, ten of which are expected to harbor an IMBH.⁴¹ This adds to the three already known in the literature: NGC 4178 Secrest et al. (2012), NGC 4713 Terashima et al. (2015), and NGC 4470 (GSD19). Collectively, this represents nearly half of our sample of 33+1 spiral galaxies expected to possess an IMBH. This contrasts notably with the 10% (central X-ray point source) detection rate in a sample of 30 Virgo cluster early-type galaxies expected to possess an IMBH (Graham & Soria 2019), even though both samples had comparable exposure times of typically more than a couple of hours per galaxy. We suggest that this outcome may not necessarily reflect the occupation fraction of IMBHs, but rather the Eddington ratios in these two samples. The amount of cool gas available is likely to be a valuable clue for future observing campaigns pursuing AGN in low-mass and dwarf galaxies. This notion also meshes with the findings from Kauffmann & Heckman (2009), which reports higher Eddington ratios in star-forming galaxies than in quiescent, i.e., non-star-forming, galaxies.

Scouring the literature, we found that four of these 14 galaxies (NGC: 4212; 4313; 4607; and 4713) have been identified as LINERs or LINER/H II composites, plus NGC 4178 has a high-ionization [Ne V] 14.32 μm emission line suggestive of an AGN. An additional two galaxies (NGC 4197 and NGC 4330) have $L_{0.5-10 \text{ keV}} \approx 10^{40} \text{ erg s}^{-1}$, making these nuclear X-ray sources likely AGN according to Lehmer et al. (2010). That is, half of our 14 late-type galaxies with a nuclear X-ray point source have evidence for hosting a massive black hole rather than a stellar-mass XRB. Furthermore, of the four (from the 11 new) galaxies for which the central X-ray emission was sufficiently strong enough to measure its spectrum (NGC 4197, NGC 4330, NGC 4492, and NGC 4607), the data favored a power law over a blackbody curve. In the case of NGC 4197, which has the brightest central X-ray point source, and for which we predict $M_{\text{bh}} = 6 \times 10^4 M_{\odot}$ (see Table 1), we found its spectrum to be consistent with the low/hard state of a greater-than-stellar-mass black hole.

We have also detected a clear, dual X-ray point source in NGC 4212, with the off-center point source located 2.9 arcsec (240 pc) away from the centrally located source. Further observation is required to establish if it is the first dual IMBH, a notion which we consider speculative but conceivable. We note that NGC 4470, NGC 4492 and NGC 4313 are also new targets of interest due to their (weaker) dual X-ray point sources, with one of each pair of point sources residing at the center of each of these galaxies, and the partner 170, 550, and 590 pc distant.




This research was supported under the Australian Research Council's funding scheme DP17012923 and the French Center National d'Etudes Spatiales (CNES) and is based upon work supported by Tamkeen under the NYU Abu Dhabi Research Institute grant CAP³. RS warmly thanks Curtin University for their hospitality during the planning stage of this project. Support for this work was provided by the National Aeronautics and Space Administration through Chandra Award Number LP18620568 issued by the Chandra X-ray Center,

which is operated by the Smithsonian Astrophysical Observatory for and on behalf of the National Aeronautics Space Administration under contract NAS8-03060. Data underlying this article are available in the Chandra Data Archive (CDA; <https://cxc.harvard.edu/cda/>), and the Next Generation Virgo Cluster Survey website (<https://www.cfht.hawaii.edu/Science/NGVS/>). Based on observations made with the NASA/ESA Hubble Space Telescope, and obtained from the Hubble Legacy Archive, which is a collaboration between the Space Telescope Science Institute (STScI/NASA), the Space Telescope European Coordinating Facility (ST-ECF/ESA), and the Canadian Astronomy Data Centre (CADM/NRC/CSA). The HST imaging data used in this paper may be obtained from the Barbara A. Mikulski Archive for Space Telescopes (MAST). This research has made use of NASA's Astrophysics Data System (ADS) Bibliographic Services and of the NASA/IPAC Extragalactic Database (NED), which is operated by the Jet Propulsion Laboratory, California Institute of Technology, under contract with NASA.

Software: IRAF (Tody 1986, 1993), *Isotfit/Cmodel* (Ciambur 2015), PROFILER (Ciambur 2016), XSPEC (v12.9.1: Arnaud 1996), CIAO (v4.12: Fruscione et al. 2006), FTOOLS (Blackburn 1995).

We thank Laura Ferrarese, Patrick Côté Jean-Charles Cuillandre, and Stephen Gwyn for access to their NGVS images.

ORCID iDs

Alister W. Graham  <https://orcid.org/0000-0002-6496-9414>
 Roberto Soria  <https://orcid.org/0000-0002-4622-796X>
 Benjamin L. Davis  <https://orcid.org/0000-0002-4306-5950>
 James Miller-Jones  <https://orcid.org/0000-0003-3124-2814>
 Christian Motch  <https://orcid.org/0000-0002-4298-5624>

References

- Abbott, B. P., Abbott, R., Abbott, T. D., et al. 2016a, *LRR*, 19, 1
 Abbott, B. P., Abbott, R., Abbott, T. D., et al. 2016b, *ApJL*, 826, L13
 Abbott, B. P., Abbott, R., Abbott, T. D., et al. 2018, *LRR*, 21, 3
 Abbott, R., Abbott, T. D., Abraham, S., et al. 2020, *PhRvL*, 125, 101102
 Abramovici, A., Althouse, W. E., Drever, R. W. P., et al. 1992, *Sci*, 256, 325
 Abramson, A., Kenney, J. D. P., Crowl, H. H., et al. 2011, *AJ*, 141, 164
 Acernese, F., Agathos, M., Agatsuma, K., et al. 2015, *CQGrA*, 32, 024001
 Alam, S., Albareti, F. D., Allende Prieto, C., et al. 2015, *ApJ*, 819, 12
 Andreoni, I., Ackley, K., Cooke, J., et al. 2017, *PASA*, 34, e069
 Armas Padilla, M., Degenaar, N., Russell, D. M., & Wijnands, R. 2013, *MNRAS*, 428, 3083
 Arnaud, K., Smith, R., & Siemiginowska, A. 2011, *Handbook of X-ray Astronomy* (Cambridge: Cambridge Univ. Press)
 Arnaud, K. A. 1996, in *ASP Conf. Ser. 101, Astronomical Data Analysis Software and Systems V*, ed. G. H. Jacoby & J. Barnes (San Francisco, CA: ASP), 17
 Aso, Y., Michimura, Y., Somiya, K., et al. 2013, *PhRvD*, 88, 043007
 Babak, S., Gair, J., Sesana, A., et al. 2017, *PhRvD*, 95, 103012
 Bachetti, M., Harrison, F. A., Walton, D. J., et al. 2014, *Natur*, 514, 202
 Bahcall, J. N., Kozlovsky, B.-Z., & Salpeter, E. E. 1972, *ApJ*, 171, 467
 Baker, J. G., Centrella, J., Choi, D.-I., et al. 2006, *ApJL*, 653, L93
 Balcells, M., Graham, A. W., Domínguez-Palmero, L., & Peletier, R. F. 2003, *ApJL*, 582, L79
 Baldassare, V. F., Geha, M., & Greene, J. 2018, *ApJ*, 868, 152
 Baldassare, V. F., Reines, A. E., Gallo, E., & Greene, J. E. 2015, *ApJL*, 809, L14
 Baldassare, V. F., Reines, A. E., Gallo, E., & Greene, J. E. 2017, *ApJ*, 850, 196
 Baldwin, J. A., Phillips, M. M., & Terlevich, R. 1981, *PASP*, 93, 5
 Ballo, L., Braitto, V., Della Ceca, R., et al. 2004, *ApJ*, 600, 634
 Barausse, E., & Lapi, A. 2020, [arXiv:2011.01994](https://arxiv.org/abs/2011.01994)
 Barazza, F. D., Binggeli, B., & Jerjen, H. 2003, *A&A*, 407, 121
 Barrows, R. S., Comerford, J. M., Greene, J. E., & Pooley, D. 2016, *ApJ*, 829, 37

⁴¹ NGC 4212 is predicted to have a black hole mass of $10^5 - (2 \times 10^6) M_{\odot}$ (GSD19).

- Barrows, R. S., Mezcua, M., & Comerford, J. M. 2019, *ApJ*, **882**, 181
- Barth, A. J., Ho, L. C., Rutledge, R. E., & Sargent, W. L. W. 2004, *ApJ*, **607**, 90
- Barth, A. J., Strigari, L. E., Bentz, M. C., Greene, J. E., & Ho, L. C. 2009, *ApJ*, **690**, 1031
- Batcheldor, D., Robinson, A., Axon, D. J., Perlman, E. S., & Merritt, D. 2010, *ApJL*, **717**, L6
- Baumgardt, H., Makino, J., & Ebisuzaki, T. 2004, *ApJ*, **613**, 1133
- Bekki, K., & Chiba, M. 2008, *ApJL*, **679**, L89
- Bekki, K., Couch, W. J., Drinkwater, M. J., & Shioya, Y. 2003, *MNRAS*, **344**, 399
- Bellovary, J. M., Cleary, C. E., Munshi, F., et al. 2019, *MNRAS*, **482**, 2913
- Bentz, M. C., Peterson, B. M., Pogge, R. W., & Vestergaard, M. 2009, *ApJL*, **694**, L166
- Bianchi, S., Chiaberge, M., Piconcelli, E., Guainazzi, M., & Matt, G. 2008, *MNRAS*, **386**, 105
- Binggeli, B., Barazza, F., & Jerjen, H. 2000, *A&A*, **359**, 447
- Binggeli, B., Sandage, A., & Tammann, G. A. 1985, *AJ*, **90**, 1681
- Birchall, K. L., Watson, M. G., & Aird, J. 2020, *MNRAS*, **492**, 2268
- Blackburn, J. K. 1995, in ASP Conf. Ser. 77, *Astronomical Data Analysis Software and Systems IV*, ed. R. A. Shaw, H. E. Payne, & J. J. E. Hayes (San Francisco, CA: ASP), 367
- Blecha, L., & Loeb, A. 2008, *MNRAS*, **390**, 1311
- Blecha, L., Sijacki, D., Kelley, L. Z., et al. 2016, *MNRAS*, **456**, 961
- Böker, T., Laine, S., van der Marel, R. P., et al. 2002, *AJ*, **123**, 1389
- Bonetti, M., & Sesana, A. 2020, *PhRvD*, **102**, 103023
- Booth, R. S., de Blok, W. J. G., Jonas, J. L., & Fanaroff, B. 2009, arXiv:0910.2935
- Boselli, A., Fossati, M., Gavazzi, G., et al. 2015, *A&A*, **579**, A102
- Brocksopp, C., Fender, R. P., Larionov, V., et al. 1999, *MNRAS*, **309**, 1063
- Brum, C., Diniz, M. R., Riffel, R. A., et al. 2019, *MNRAS*, **486**, 691
- Burbidge, G. R. 1970, *ARA&A*, **8**, 369
- Burke, C. J., Shen, Y., Blaes, O., et al. 2021, *Sci*, **373**, 789
- Burke-Spolaor, S. 2011, *MNRAS*, **410**, 2113
- Burke-Spolaor, S., Blecha, L., Bogdanović, T., et al. 2018, in ASP Conf. Ser. 517, *Science with a Next Generation Very Large Array*, ed. E. Murphy (San Francisco, CA: ASP), 677
- Campanelli, M., Lousto, C., Zlochower, Y., & Merritt, D. 2007, *ApJL*, **659**, L5
- Cann, J. M., Satyapal, S., Abel, N. P., et al. 2019, *ApJL*, **870**, L2
- Cann, J. M., Satyapal, S., Rothberg, B., et al. 2021, *ApJL*, **912**, L2
- Capetti, A., Kharb, P., Axon, D. J., Merritt, D., & Baldi, R. D. 2009, *AJ*, **138**, 1990
- Carilli, C. L., McKinnon, M., Ott, J., et al. 2015, arXiv:1510.06438
- Carollo, C. M., Stiavelli, M., de Zeeuw, P. T., & Mack, J. 1997, *AJ*, **114**, 2366
- Caron, B., Dominjon, A., Drezzen, C., et al. 1997, *CQGra*, **14**, 1461
- Casares, J., Charles, P. A., & Naylor, T. 1992, *Natur*, **355**, 614
- Casares, J., Negueruela, I., Ribó, M., et al. 2014, *Natur*, **505**, 378
- Cash, W. 1979, *ApJ*, **228**, 939
- Chilingarian, I. V., Katkov, I. Y., Zolotukhin, I. Y., et al. 2018, *ApJ*, **863**, 1
- Chilingarian, I. V., Zolotukhin, I. Y., Katkov, I. Y., et al. 2017, *ApJS*, **228**, 14
- Choi, Y., Gibson, R. R., Becker, A. C., et al. 2014, *ApJ*, **782**, 37
- Chung, A., van Gorkom, J. H., Kenney, J. D. P., & Vollmer, B. 2007, *ApJL*, **659**, L115
- Ciambur, B. C. 2015, *ApJ*, **810**, 120
- Ciambur, B. C. 2016, *PASA*, **33**, e062
- Cid Fernandes, R., Stasińska, G., Mateus, A., & Vale Asari, N. 2011, *MNRAS*, **413**, 1687
- Civano, F., Elvis, M., Lanzuisi, G., et al. 2010, *ApJ*, **717**, 209
- Cloet-Osselaer, A., De Rijcke, S., Vandenbroucke, B., et al. 2014, *MNRAS*, **442**, 2909
- Comerford, J. M., Gerke, B. F., Newman, J. A., et al. 2009b, *ApJ*, **698**, 956
- Comerford, J. M., Griffith, R. L., Gerke, B. F., et al. 2009a, *ApJL*, **702**, L82
- Comerford, J. M., Pooley, D., Barrows, R. S., et al. 2015, *ApJ*, **806**, 219
- Conselice, C. J., Bhatwadekar, R., Palmese, A., & Hartley, W. G. 2020, *ApJ*, **890**, 8
- Corbel, S., Nowak, M. A., Fender, R. P., Tzioumis, A. K., & Markoff, S. 2003, *A&A*, **400**, 1007
- Corral, A., Della Ceca, R., Caccianiga, A., et al. 2011, *A&A*, **530**, A42
- Côté, P., Blakeslee, J. P., Ferrarese, L., et al. 2004, *ApJS*, **153**, 223
- Côté, P., Piatek, S., Ferrarese, L., et al. 2006, *ApJS*, **165**, 57
- Coughlin, M. W., Ahumada, T., Anand, S., et al. 2019, *ApJL*, **885**, L19
- Dahari, O. 1985, *ApJS*, **57**, 643
- Dale, D. A., Smith, J. D. T., Armus, L., et al. 2006, *ApJ*, **646**, 161
- Danzmann, K. & LISA Study Team 1997, *CQGra*, **14**, 1399
- Davies, J. I., Phillipps, S., Cawson, M. G. M., Disney, M. J., & Kibblewhite, E. J. 1988, *MNRAS*, **232**, 239
- Davis, B. L., & Graham, A. W. 2021, *PASA*, **38**, e030
- Davis, B. L., Graham, A. W., & Cameron, E. 2018, *ApJ*, **869**, 113
- Davis, B. L., Graham, A. W., & Cameron, E. 2019, *ApJ*, **873**, 85
- Davis, B. L., Graham, A. W., & Seigar, M. S. 2017, *MNRAS*, **471**, 2187
- Davis, T. A., Nguyen, D. D., Seth, A. C., et al. 2020, *MNRAS*, **496**, 4061
- Decarli, R., Gavazzi, G., Arosio, I., et al. 2007, *MNRAS*, **381**, 136
- den Brok, M., Seth, A. C., Barth, A. J., et al. 2015, *ApJ*, **809**, 101
- Dewdney, P. E., Hall, P. J., Schilizzi, R. T., & Lazio, T. J. L. W. 2009, in Proc. IEEE, 97 (Piscataway, NJ: IEEE), 1482
- Doi, A., Asada, K., Fujisawa, K., et al. 2013, *ApJ*, **765**, 69
- Dokuchaev, V. I., & Ozernoi, L. M. 1981, *SvAL*, **7**, 158
- Dong, A.-J., & Wu, Q. 2015, *MNRAS*, **453**, 3447
- Dong, X., Wang, T., Yuan, W., et al. 2007, *ApJ*, **657**, 700
- Dubus, G., Charles, P. A., & Long, K. S. 2004, *A&A*, **425**, 95
- Dubus, G., & Rutledge, R. E. 2002, *MNRAS*, **336**, 901
- Fabbiano, G., Paggi, A., Karovska, M., et al. 2020, *ApJ*, **902**, 49
- Falcke, H., Körding, E., & Markoff, S. 2004, *A&A*, **414**, 895
- Farinelli, R., Ferrigno, C., Bozzo, E., & Becker, P. A. 2016, *A&A*, **591**, A29
- Farrell, S. A., Webb, N. A., Barret, D., Godet, O., & Rodrigues, J. M. 2009, *Natur*, **460**, 73
- Feng, H., & Soria, R. 2011, *NewAR*, **55**, 166
- Ferrarese, L., Côté, P., Cuillandre, J.-C., et al. 2012, *ApJS*, **200**, 4
- Ferrarese, L., Côté, P., Jordán, A., et al. 2006, *ApJS*, **164**, 334
- Ferrigno, C., Becker, P. A., Segreto, A., Mineo, T., & Santangelo, A. 2009, *A&A*, **498**, 825
- Filho, M. E., Barthel, P. D., & Ho, L. C. 2002, *ApJS*, **142**, 223
- Filippenko, A. V., & Sargent, W. L. W. 1985, *ApJS*, **57**, 503
- Fischer, T. C., Secrest, N. J., Johnson, M. C., et al. 2021, *ApJ*, **906**, 88
- Fish, V., Akiyama, K., Bouman, K., et al. 2016, *Galax*, **4**, 54
- Foschini, L., Rodriguez, J., Fuchs, Y., et al. 2004, *A&A*, **416**, 529
- Fossati, M., Mendel, J. T., Boselli, A., et al. 2018, *A&A*, **614**, A57
- Fragos, T., Lehmer, B., Tremmel, M., et al. 2013, *ApJ*, **764**, 41
- Frank, J., & Rees, M. J. 1976, *MNRAS*, **176**, 633
- Fruscione, A., McDowell, J. C., Allen, G. E., et al. 2006, *Proc. SPIE*, **6270**, 62701V
- Fu, H., Zhang, Z.-Y., Assef, R. J., et al. 2011, *ApJL*, **740**, L44
- Gair, J. R., Barack, L., Creighton, T., et al. 2004, *CQGra*, **21**, S1595
- Gair, J. R., Mandel, I., Miller, M. C., & Volonteri, M. 2011, *GRGr*, **43**, 485
- Galletti, S., Federici, L., Bellazzini, M., Fusi Pecci, F., & Macrina, S. 2004, *A&A*, **416**, 917
- Gallo, E., Treu, T., Jacob, J., et al. 2008, *ApJ*, **680**, 154
- Gallo, E., Treu, T., Marshall, P. J., et al. 2010, *ApJ*, **714**, 25
- Garofali, K., Converse, J. M., Chandar, R., & Rangelov, B. 2012, *ApJ*, **755**, 49
- Gaskin, J. A., Swartz, D. A., Vikhlinin, A., et al. 2019, *JATIS*, **5**, 021001
- Georgiev, I. Y., & Böker, T. 2014, *MNRAS*, **441**, 3570
- Georgiev, I. Y., Böker, T., Leigh, N., Lützgendorf, N., & Neumayer, N. 2016, *MNRAS*, **457**, 2122
- González Delgado, R. M., Pérez, E., Cid Fernandes, R., & Schmitt, H. 2008, *AJ*, **135**, 747
- González Delgado, R. M., Pérez, E., Tadhunter, C., Vilchez, J. M., & José Miguel Rodríguez-Espinoza, A. 1997, *ApJS*, **108**, 155
- Graham, A. W. 2016, in IAU Symp. 312, *Star Clusters and Black Holes in Galaxies across Cosmic Time*, ed. Y. Meiron et al. (Cambridge: Cambridge Univ. Press), 269
- Graham, A. W. 2020, *MNRAS*, **492**, 3263
- Graham, A. W., Ciambur, B. C., & Soria, R. 2016, *ApJ*, **818**, 172
- Graham, A. W., & Driver, S. P. 2005, *PASA*, **22**, 118
- Graham, A. W., & Driver, S. P. 2007, *ApJ*, **655**, 77
- Graham, A. W., & Guzmán, R. 2003, *AJ*, **125**, 2936
- Graham, A. W., Onken, C. A., Athanassoula, E., & Combes, F. 2011, *MNRAS*, **412**, 2211
- Graham, A. W., & Scott, N. 2015, *ApJ*, **798**, 54
- Graham, A. W., & Soria, R. 2019, *MNRAS*, **484**, 794
- Graham, A. W., Soria, R., Ciambur, B. C., Davis, B. L., & Swartz, D. A. 2021, *ApJ*, **923**, 146
- Graham, A. W., Soria, R., & Davis, B. L. 2019, *MNRAS*, **484**, 814
- Graham, A. W., & Spitler, L. R. 2009, *MNRAS*, **397**, 2148
- Graham, A. W., Spitler, L. R., Forbes, D. A., et al. 2012, *ApJ*, **750**, 121
- Graham, A. W., & Worley, C. C. 2008, *MNRAS*, **388**, 1708
- GRAVITY Collaboration, Abuter, R., Amorim, A., et al. 2021, *A&A*, **645**, A127
- Green, J., Van Langevelde, H. J., Brunthaler, A., et al. 2015, *PoS*, **AASKA14**, 119
- Greene, J. E., & Ho, L. C. 2007, *ApJ*, **670**, 92
- Greenhill, L. J., Kondratko, P. T., Lovell, J. E. J., et al. 2003, *ApJL*, **582**, L11
- Grogin, N. A., Geller, M. J., & Huchra, J. P. 1998, *ApJS*, **119**, 277

- Guinazzi, M., Piconcelli, E., Jiménez-Bailón, E., & Matt, G. 2005, *A&A*, **429**, L9
- Gültekin, K., Cackett, E. M., Miller, J. M., et al. 2009, *ApJ*, **706**, 404
- Gültekin, K., King, A. L., Cackett, E. M., et al. 2019, *ApJ*, **871**, 80
- Gursky, H., Kellogg, E. M., Leong, C., Tananbaum, H., & Giacconi, R. 1971, *ApJL*, **165**, L43
- Hannikainen, D. C., Hunstead, R. W., Campbell-Wilson, D., & Sood, R. K. 1998, *A&A*, **337**, 460
- Harrison, F. A., Craig, W. W., Christensen, F. E., et al. 2013, *ApJ*, **770**, 103
- Harry, G. M. & LIGO Scientific Collaboration 2010, *CQGra*, **27**, 084006
- Herrmann, F., Hinder, I., Shoemaker, D., Laguna, P., & Matzner, R. A. 2007, *ApJ*, **661**, 430
- HI4PI Collaboration, Ben Bekhti, N., Flöer, L., et al. 2016, *A&A*, **594**, A116
- Ho, L. C., Filippenko, A. V., & Sargent, W. L. 1995, *ApJS*, **98**, 477
- Ho, L. C., Filippenko, A. V., & Sargent, W. L. W. 1997, *ApJS*, **112**, 315
- Ho, L. C., Greene, J. E., Filippenko, A. V., & Sargent, W. L. W. 2009, *ApJS*, **183**, 1
- Homan, J., & Belloni, T. 2005, *Ap&SS*, **300**, 107
- Horner, S. D., & Rieke, M. J. 2004, *Proc. SPIE*, **5487**, 628
- Hough, D. H., Vermeulen, R. C., Readhead, A. C. S., et al. 2002, *AJ*, **123**, 1258
- Huerta, E. A., & Gair, J. R. 2011, *PhRvD*, **83**, 044020
- Humphreys, E. M. L., Vlemmings, W. H. T., Impellizzeri, C. M. V., et al. 2016, *A&A*, **592**, L13
- Illarionov, A. F., & Romanova, M. M. 1988, *AZh*, **65**, 682
- Ishikawa, T., Iwaguchi, S., Michimura, Y., et al. 2021, *Galax*, **9**, 14
- Ivezić, Ž., Brandt, W. N., Fan, X., et al. 2014, in *IAU Symp.* 304, Multiwavelength AGN Surveys and Studies, ed. A. M. Mickaelian & D. B. Sanders (Cambridge: Cambridge Univ. Press), 11
- Janssen, M., Falcke, H., Kadler, M., et al. 2021, *NatAs*, **5**, 1017
- Jerjen, H., Binggeli, B., & Freeman, K. C. 2000, *AJ*, **119**, 593
- Jiang, N., Wang, T., Zhou, H., et al. 2018, *ApJ*, **869**, 49
- Johns Mulia, P., Chandar, R., & Rangelov, B. 2019, *ApJ*, **871**, 122
- Jonas, J. L. 2009, in *Proc. IEEE*, 97 (Piscataway, NJ: IEEE) 1522
- Kaaret, P., Feng, H., & Roberts, T. P. 2017, *ARA&A*, **55**, 303
- Karachentsev, I. D., Karachentseva, V. E., & Parnovskij, S. L. 1993, *AN*, **314**, 97
- Kauffmann, G., & Heckman, T. M. 2009, *MNRAS*, **397**, 135
- Kawamura, S., Ando, M., Seto, N., et al. 2011, *CQGra*, **28**, 094011
- Kewley, L. J., Groves, B., Kauffmann, G., & Heckman, T. 2006, *MNRAS*, **372**, 961
- Kim, D. C., Yoon, I., Privon, G. C., et al. 2017, *ApJ*, **840**, 71
- Kim, D.-W., & Fabbiano, G. 2004, *ApJ*, **611**, 846
- Kim, D. W., Fabbiano, G., Ivanova, N., et al. 2013, *ApJ*, **764**, 98
- Komossa, S., Burwitz, V., Hasinger, G., et al. 2003, *ApJL*, **582**, L15
- Komossa, S., & Merritt, D. 2008, *ApJL*, **689**, L89
- Komossa, S., Ciprini, S., Dey, L., et al. 2021, *POBeo*, **100**, 29
- Koposov, S. E., Boubert, D., Li, T. S., et al. 2020, *MNRAS*, **491**, 2465
- Kosec, P., Brightman, M., Stern, D., et al. 2017, *ApJ*, **850**, 168
- Kraft, R. P., Burrows, D. N., & Nousek, J. A. 1991, *ApJ*, **374**, 344
- Krivonos, R., Sazonov, S., Tsygankov, S. S., & Poutanen, J. 2018, *MNRAS*, **480**, 2357
- Kuo, C. Y., Braatz, J. A., Condon, J. J., et al. 2011, *ApJ*, **727**, 20
- La Franca, F., Onori, F., Ricci, F., et al. 2015, *MNRAS*, **449**, 1526
- La Parola, V., D'Ai, A., Cusumano, G., & Mineo, T. 2015, *A&A*, **580**, A71
- Lamperti, I., Koss, M., Trakhtenbrot, B., et al. 2017, *MNRAS*, **467**, 540
- Larkin, J. E., Moore, A. M., Wright, S. A., et al. 2016, *Proc. SPIE*, **9908**, 99081W
- Larsen, S. S., Romanowsky, A. J., Brodie, J. P., & Wasserman, A. 2020, *Sci*, **370**, 970
- Lehmer, B. D., Alexander, D. M., Bauer, F. E., et al. 2010, *ApJ*, **724**, 559
- Lehmer, B. D., Eufrazio, R. T., Tzanavaris, P., et al. 2019, *ApJS*, **243**, 3
- Lehmer, B. D., Ferrell, A. P., Doore, K., et al. 2020, *ApJS*, **248**, 31
- Lena, D., Robinson, A., Marconi, A., et al. 2014, *ApJ*, **795**, 146
- Levin, Y. 2006, *ApJ*, **653**, 1203
- Li, D., Nan, R., & Pan, Z. 2013, in *IAU Symp.* 291, Neutron Stars and Pulsars: Challenges and Opportunities after 80 yr, ed. J. van Leeuwen (Cambridge: Cambridge Univ. Press), 325
- Li, K., Ballantyne, D. R., & Bogdanović, T. 2021, *ApJ*, **916**, 110
- Li, K., Bogdanović, T., & Ballantyne, D. R. 2020, *ApJ*, **896**, 113
- Lin, D., Strader, J., Romanowsky, A. J., et al. 2020, *ApJL*, **892**, L25
- Liu, H.-Y., Yuan, W., Dong, X.-B., Zhou, H., & Liu, W.-J. 2018, *ApJS*, **235**, 40
- Liu, T., Gezari, S., Ayers, M., et al. 2019, *ApJ*, **884**, 36
- Liu, X., Han, Z., & Zhang, Z. 2016, *Ap&SS*, **361**, 9
- Lusso, E., Comastri, A., Simmons, B. D., et al. 2012, *MNRAS*, **425**, 623
- Lynden-Bell, D. 1969, *Natur*, **223**, 690
- Makarov, D., & Karachentsev, I. 2011, *MNRAS*, **412**, 2498
- Manzano-King, C. M., Canalizo, G., & Sales, L. V. 2019, *ApJ*, **884**, 54
- Mapelli, M., Dall'Amico, M., Bouffanais, Y., et al. 2021, *MNRAS*, **505**, 339
- Mapelli, M., Ripamonti, E., Vecchio, A., Graham, A. W., & Gualandris, A. 2012, *A&A*, **542**, A102
- Martínez-Palomera, J., Lira, P., Bhalla-Ladd, I., Förster, F., & Plotkin, R. M. 2020, *ApJ*, **889**, 113
- Matthews, L. D., Gallagher, J. S. I., Krist, J. E., et al. 1999, *AJ*, **118**, 208
- McDermid, R. M., Cresci, G., Rigaut, F., et al. 2020, arXiv:2009.09242
- McGregor, P. J., Bloxham, G. J., Boz, R., et al. 2012, *Proc. SPIE*, **8446**, 844611
- McGurk, R. C., Max, C. E., Medling, A. M., Shields, G. A., & Comerford, J. M. 2015, *ApJ*, **811**, 14
- Menezes, R. B., Steiner, J. E., & Ricci, T. V. 2014, *ApJL*, **796**, L13
- Merloni, A., Heinz, S., & di Matteo, T. 2003, *MNRAS*, **345**, 1057
- Merritt, D. 2013, *Dynamics and Evolution of Galactic Nuclei* (Princeton: Princeton Univ. Press)
- Merritt, D. 2015, *ApJ*, **814**, 57
- Merritt, D., & Ferrarese, L. 2001, in *ASP Conf. Ser.* 249, The Central Kiloparsec of Starbursts and AGN, ed. J. H. Knapen et al. (San Francisco: ASP), 335
- Merritt, D., & Milosavljević, M. 2005, *LRR*, **8**, 8
- Merritt, D., Milosavljević, M., Favata, M., Hughes, S. A., & Holz, D. E. 2004, *ApJL*, **607**, L9
- Merritt, D., Schnittman, J. D., & Komossa, S. 2009, *ApJ*, **699**, 1690
- Mezcua, M., Civano, F., Marchesi, S., et al. 2018, *MNRAS*, **478**, 2576
- Mezcua, M., & Domínguez Sánchez, H. 2020, *ApJL*, **898**, L30
- Middleton, M. J., Sutton, A. D., & Roberts, T. P. 2011, *MNRAS*, **417**, 464
- Mineo, S., Gilfanov, M., & Sunyaev, R. 2012, *MNRAS*, **419**, 2095
- Miyoshi, M., Moran, J., Herrnstein, J., et al. 1995, *Natur*, **373**, 127
- Molina, M., Bassani, L., Malizia, A., et al. 2009, *MNRAS*, **399**, 1293
- Monty, S., Rigaut, F., McDermid, R., et al. 2021, *MNRAS*, **507**, 2192
- Morales, G., Martínez-Delgado, D., Grebel, E. K., et al. 2018, *A&A*, **614**, A143
- Moran, E. C., Shahinyan, K., Sugarman, H. R., Vélez, D. O., & Eracleous, M. 2014, *AJ*, **148**, 136
- Motta, S., Belloni, T., & Homan, J. 2009, *MNRAS*, **400**, 1603
- Mushotzky, R. 2018, *Proc. SPIE*, **10699**, 1069929
- Nagar, N. M., Falcke, H., & Wilson, A. S. 2005, *A&A*, **435**, 521
- Nan, R. 2006, *ScChG*, **49**, 129
- Nandra, K., Barret, D., Barcons, X., et al. 2013, arXiv:1306.2307
- Narayan, R., & Yi, I. 1995, *ApJ*, **452**, 710
- Nguyen, D. D., Seth, A. C., den Brok, M., et al. 2017, *ApJ*, **836**, 237
- Nguyen, D. D., Seth, A. C., Neumayer, N., et al. 2018, *ApJ*, **858**, 118
- Nguyen, D. D., Seth, A. C., Neumayer, N., et al. 2019, *ApJ*, **872**, 104
- Nisbet, D. M., & Best, P. N. 2016, *MNRAS*, **455**, 2551
- Nowak, N., Saglia, R. P., Thomas, J., et al. 2007, *MNRAS*, **379**, 909
- Oka, T., Tsujimoto, S., Iwata, Y., Nomura, M., & Takekawa, S. 2017, *NatAs*, **1**, 709
- Onken, C. A., Ferrarese, L., Merritt, D., et al. 2004, *ApJ*, **615**, 645
- Onken, C. A., Valluri, M., Brown, J. S., et al. 2014, *ApJ*, **791**, 37
- Paragi, Z., Godfrey, L., Reynolds, C., et al. 2015, in *PoS (AASKA14)*, 215 (Trieste: SISSA) 143
- Pastorini, G., Marconi, A., Capetti, A., et al. 2007, *A&A*, **469**, 405
- Paturel, G., Petit, C., Prugniel, P., et al. 2003, *A&A*, **412**, 45
- Paudel, S., Smith, R., Yoon, S. J., Calderón-Castillo, P., & Duc, P.-A. 2018, *ApJS*, **237**, 36
- Peebles, P. J. E. 1972, *ApJ*, **178**, 371
- Penny, S. J., Masters, K. L., Smethurst, R., et al. 2018, *MNRAS*, **476**, 979
- Pestoni, B., Bortolas, E., Capelo, P. R., & Mayer, L. 2021, *MNRAS*, **500**, 4628
- Peterson, B. M., Korista, K. T., & Cota, S. A. 1987, *ApJL*, **312**, L1
- Peterson, B. M., & Wandel, A. 2000, *ApJL*, **540**, L13
- Peterson, B. M., Ferrarese, L., Gilbert, K. M., et al. 2004, *ApJ*, **613**, 682
- Pfister, H., Volonteri, M., Dai, J. L., & Colpi, M. 2020, *MNRAS*, **497**, 2276
- Pfister, H., Volonteri, M., Dubois, Y., Dotti, M., & Colpi, M. 2019, *MNRAS*, **486**, 101
- Pintore, F., Zampieri, L., Stella, L., et al. 2017, *ApJ*, **836**, 113
- Plotkin, R. M., Gallo, E., & Jonker, P. G. 2013, *ApJ*, **773**, 59
- Plotkin, R. M., Markoff, S., Kelly, B. C., Körding, E., & Anderson, S. F. 2012, *MNRAS*, **419**, 267
- Plotkin, R. M., Miller-Jones, J. C. A., Gallo, E., et al. 2017, *ApJ*, **834**, 104
- Pounds, K. A., Nandra, K., Stewart, G. C., George, I. M., & Fabian, A. C. 1990, *Natur*, **344**, 132
- Pringle, J. E., & Rees, M. J. 1972, *A&A*, **21**, 1
- Punturo, M., Abernathy, M., Acernese, F., et al. 2010, *CQGra*, **27**, 194002
- Quinlan, G. D., & Shapiro, S. L. 1990, *ApJ*, **356**, 483

- Radcliffe, J. F., Barthel, P. D., Garrett, M. A., et al. 2021, *A&A*, **649**, L9
- Rau, A., Meidinger, N., Nandra, K., et al. 2013, arXiv:1308.6785
- Ravi, V., Vedantham, H., & Phinney, E. S. 2018, *MNRAS*, **478**, L72
- Reaves, G. 1983, *ApJS*, **53**, 375
- Reines, A. E., Condon, J. J., Darling, J., & Greene, J. E. 2020, *ApJ*, **888**, 36
- Reines, A. E., Greene, J. E., & Geha, M. 2013, *ApJ*, **775**, 116
- Reitze, D., Adhikari, R. X., Ballmer, S., et al. 2019, *BAAS*, **51**, 35
- Rodriguez, C., Taylor, G. B., Zavala, R. T., et al. 2006, *ApJ*, **646**, 49
- Roediger, J. C., & Courteau, S. 2015, *MNRAS*, **452**, 3209
- Rubin, V. 1974, *Nuclei of Galaxies, Black Holes, and Collapsed Matter* (3rd; Erice, Italy: Center for Scientific Culture), 11
- Rubinur, K., Kharb, P., Das, M., et al. 2021, *MNRAS*, **500**, 3908
- Russell, T. D., White, R. L., Long, K. S., et al. 2020, *MNRAS*, **495**, 479
- Sahu, N., Graham, A. W., & Davis, B. L. 2019a, *ApJ*, **876**, 155
- Sahu, N., Graham, A. W., & Davis, B. L. 2019b, *ApJ*, **887**, 10
- Sandage, A., Binggeli, B., & Tammann, G. A. 1985, *AJ*, **90**, 1759
- Sanders, R. H., & Lowinger, T. 1972, *AJ*, **77**, 292
- Sarajedini, V. L., Gilliland, R. L., & Kasm, C. 2003, *ApJ*, **599**, 173
- Sarajedini, V. L., Koo, D. C., Phillips, A. C., et al. 2006, *ApJS*, **166**, 69
- Sartori, L. F., Schawinski, K., Treister, E., et al. 2015, *MNRAS*, **454**, 3722
- Satyapal, S., Böker, T., Mcalpine, W., et al. 2009, *ApJ*, **704**, 439
- Scarlata, C., Stiavelli, M., Hughes, M. A., et al. 2004, *AJ*, **128**, 1124
- Scott, N., & Graham, A. W. 2013, *ApJ*, **763**, 76
- Secrest, N. J., Satyapal, S., Gliozzi, M., et al. 2012, *ApJ*, **753**, 38
- Sérsic, J. L. 1973, *PASP*, **85**, 103
- Sesana, A., Haardt, F., & Madau, P. 2006, *ApJ*, **651**, 392
- Seth, A., Agüeros, M., Lee, D., & Basu-Zych, A. 2008, *ApJ*, **678**, 116
- Shen, Y., Hwang, H.-C., Zakamska, N., & Liu, X. 2019, *ApJL*, **885**, L4
- Silk, J. 2017, *ApJL*, **839**, L13
- Sivakoff, G. R., Jordán, A., Sarazin, C. L., et al. 2007, *ApJ*, **660**, 1246
- Smith, S. 1935, *ApJ*, **82**, 192
- Sobolewska, M. A., Papadakis, I. E., Done, C., & Malzac, J. 2011, *MNRAS*, **417**, 280
- Soria, R., Kolehmainen, M., Graham, A. W., et al. 2021, *MNRAS*, submitted
- Soria, R., & Wu, K. 2003, *A&A*, **410**, 53
- Stern, D., Assef, R. J., Benford, D. J., et al. 2012, *ApJ*, **753**, 30
- Strader, J., Chomiuk, L., Maccarone, T. J., et al. 2012, *ApJL*, **750**, L27
- Subramanian, S., Ramya, S., Das, M., et al. 2016, *MNRAS*, **455**, 3148
- Sundararajan, P. A., Khanna, G., & Hughes, S. A. 2010, *PhRvD*, **81**, 104009
- Sutton, A. D., Roberts, T. P., Gladstone, J. C., & Walton, D. J. 2015, *MNRAS*, **450**, 787
- Terashima, Y., Hirata, Y., Awaki, H., et al. 2015, *ApJ*, **814**, 11
- Terzić, B., & Graham, A. W. 2005, *MNRAS*, **362**, 197
- Thatte, N. A., Clarke, F., Bryson, I., et al. 2016, *Proc. SPIE*, **9908**, 99081X
- The Event Horizon Telescope Collaboration, Akiyama, K., Alberdi, A., et al. 2019, *ApJL*, **875**, L4
- Thornton, C. E., Barth, A. J., Ho, L. C., Rutledge, R. E., & Greene, J. E. 2008, *ApJ*, **686**, 892
- Tingay, S. J., Jauncey, D. L., Reynolds, J. E., et al. 2000, *AJ*, **119**, 1695
- Tody, D. 1986, *Proc. SPIE*, **627**, 733
- Tody, D. 1993, in *ASP Conf. Ser. 52, Astronomical Data Analysis Software and Systems II*, ed. R. J. Hanisch, R. J. V. Brissenden, & J. Barnes (San Francisco, CA: ASP), 173
- Tonry, J. L. 1984, *ApJL*, **283**, L27
- Tremaine, S. D., Ostriker, J. P., & Spitzer, L. J. 1975, *ApJ*, **196**, 407
- Tremmel, M., Governato, F., Volonteri, M., Pontzen, A., & Quinn, T. R. 2018, *ApJL*, **857**, L22
- Tremou, E., Strader, J., Chomiuk, L., et al. 2018, *ApJ*, **862**, 16
- Tubín, D., Treister, E., D'Ago, G., et al. 2021, *ApJ*, **911**, 100
- Tzanavaris, P., & Georgantopoulos, I. 2007, *A&A*, **468**, 129
- Valencia-S., M., Zuther, J., Eckart, A., et al. 2012, *A&A*, **544**, A129
- van Haarlem, M. P., Wise, M. W., Gunst, A. W., et al. 2013, *A&A*, **556**, A2
- Veilleux, S., & Osterbrock, D. E. 1987, *ApJS*, **63**, 295
- Vollmer, B., Soida, M., Braine, J., et al. 2012, *A&A*, **537**, A143
- Wan, Z., Lewis, G. F., Li, T. S., et al. 2020, *Natur*, **583**, 768
- Wang, S., Liu, J., Qiu, Y., et al. 2016, *ApJS*, **224**, 40
- Werner, M. W., Roellig, T. L., Low, F. J., et al. 2004, *ApJS*, **154**, 1
- Wilkins, S. M., Gonzalez-Perez, V., Baugh, C. M., Lacey, C. G., & Zuntz, J. 2013, *MNRAS*, **431**, 430
- Willmer, C. N. A. 2018, *ApJS*, **236**, 47
- Wood, K. S., Meekins, J. F., Yentis, D. J., et al. 1984, *ApJS*, **56**, 507
- Woodgate, B. E., Kimble, R. A., Bowers, C. W., et al. 1998, *PASP*, **110**, 1183
- Wright, E. L., Eisenhardt, P. R. M., Mainzer, A. K., et al. 2010, *AJ*, **140**, 1868
- Yang, Q.-X., Xie, F.-G., Yuan, F., et al. 2015, *MNRAS*, **447**, 1692
- Yao, H. F. M., Jarrett, T. H., Cluver, M. E., et al. 2020, *ApJ*, **903**, 91
- Young, C. K., & Currie, M. J. 1994, *MNRAS*, **268**, L11
- Yozin, C., & Bekki, K. 2012, *ApJL*, **756**, L18
- Yuan, W., Zhou, H., Dou, L., et al. 2014, *ApJ*, **782**, 55
- Zackay, B., Dai, L., Venumadhav, T., Roulet, J., & Zaldarriaga, M. 2021, *PhRvD*, **104**, 063030
- Zaw, I., Rosenthal, M. J., Katkov, I. Y., et al. 2020, *ApJ*, **897**, 111
- Zezas, A., Birkinshaw, M., Worrall, D. M., Peters, A., & Fabbiano, G. 2005, *ApJ*, **627**, 711
- Zhang, H.-X., Paudel, S., Smith, R., et al. 2020, *ApJL*, **891**, L23
- Zhang, Z., Gilfanov, M., & Bogdán, Á. 2012, *A&A*, **546**, A36
- Zhou, H., Wang, T., Zhang, X., Dong, X., & Li, C. 2004, *ApJL*, **604**, L33